JGP Journal of General Physiology

RESEARCH ARTICLE

Effects of FGF14 and $Na_V\beta4$ deletion on transient and resurgent Na current in cerebellar Purkinje neurons

Hayley V. White[1,2], Spencer T. Brown[1,2], Thomas C. Bozza[1,2], and Indira M. Raman[1,2]

Voltage-gated Na channels of Purkinje cells are specialized to maintain high availability during high-frequency repetitive firing. They enter fast-inactivated states relatively slowly and undergo a voltage-dependent open-channel block by an intracellular protein (or proteins) that prevents stable fast inactivation and generates resurgent Na current. These properties depend on the pore-forming α subunits, as well as modulatory subunits within the Na channel complex. The identity of the factors responsible for open-channel block remains a question. Here we investigate the effects of genetic mutation of two Na channel auxiliary subunits highly expressed in Purkinje cells, $Na_V\beta4$ and FGF14, on modulating Na channel blocked as well as inactivated states. We find that although both $Na_V\beta4$ and the FGF14 splice variant FGF14-1a contain sequences that can generate resurgent-like currents when applied to Na channels in peptide form, deletion of either protein, or both proteins simultaneously, does not eliminate resurgent current in acutely dissociated Purkinje cell bodies. Loss of FGF14 expression does, however, reduce resurgent current amplitude and leads to an acceleration and stabilization of inactivation that is not reversed by application of the site-3 toxin, anemone toxin II (ATX). Tetrodotoxin (TTX) sensitivity is higher for resurgent than transient components of Na current, and loss of FGF14 preferentially affects a highly TTX-sensitive subset of Purkinje α subunits. The data suggest that $Na_V1.6$ channels, which are known to generate the majority of Purkinje cell resurgent current, bind TTX with high affinity and are modulated by FGF14 to facilitate open-channel block.

Introduction

Voltage-gated Na current is required for the upstroke of the action potential in nearly all neurons. Consequently, action potential firing frequencies depend on the availability of Na channels to open upon depolarization, which is set by the rates of entry into and recovery from nonconducting channel states. These rates vary with the identity of the pore-forming α subunit, as well as with the auxiliary subunits that compose Na channel complexes. For instance, cerebellar Purkinje cells, which have several ion channels specialized for rapid firing (Raman and Bean, 1999; Khaliq et al., 2003; Martina et al., 2007; Carter and Bean, 2009, 2011; Benton et al., 2013), have Na channels well suited to maintain high availability. They express a high proportion of $Na_V1.6$ subunits (gene *scn8a*), which show less stable inactivation, faster recovery from inactivation, and less slow inactivation than other α subunits (Raman et al., 1997; Smith et al., 1998; Herzog et al., 2003; Do and Bean, 2004; Aman and Raman, 2007; Mercer et al., 2007).

Purkinje cells also express auxiliary proteins that further increase Na channel availability. One such protein acts as a voltage-dependent intracellular open-channel blocking particle that competes with fast inactivation (Raman et al., 1997; Raman and Bean, 2001; Grieco et al., 2002, 2005; Grieco and Raman, 2004). Unlike the inactivation gate within the DIII-DIV linker (Eaholtz et al., 1994; Yan et al., 2017; Pan et al., 2018; Shen et al., 2019), this protein binds in the permeation pathway upon depolarization and is expelled by permeating ions upon repolarization, before activation gates close (Afshari et al., 2004; Aman and Raman, 2010). Under voltage clamp, Na channels with this protein produce transient current upon depolarization followed by resurgent current upon repolarization; during spiking, unblocking rapidly restores availability, facilitating high-frequency firing (Raman and Bean, 1997, 2001; Khaliq et al., 2003; Aman and Raman, 2007; Lewis and Raman, 2014).

The molecular identity of the proteins that determine the balance between open-channel block and fast inactivation

[1]Department of Neurobiology, Northwestern University, Evanston, IL; [2]Northwestern University Interdepartmental Neuroscience Program, Northwestern University, Evanston, IL.

Correspondence to Indira M. Raman: i-raman@northwestern.edu.

remains a question. To date, the best candidate for the blocking protein is the Na channel subunit $Na_V\beta4$ (gene *scn4b*, Yu et al., 2003), since a "β4 peptide" from the $Na_V\beta4$ cytoplasmic tail induces a resurgent-like current in cells lacking a native blocker (Grieco et al., 2005). Heterologous expression of $Na_V\beta4$ with pore-forming subunits, however, cannot reconstitute resurgent current (Chen et al., 2008; Aman et al., 2009; Theile et al., 2011). Additionally, when $Na_V\beta4$ expression is reduced or abolished in cerebellar granule cells, dorsal root ganglion (DRG) neurons, or Purkinje cells (Bant and Raman, 2010; Barbosa et al., 2015; Ransdell et al., 2017), resurgent current is decreased but not eliminated, raising the question of what other proteins directly or indirectly influence open-channel block.

A second auxiliary protein that is well positioned to regulate Na channel availability is intracellular fibroblast growth factor homologous factor 14 (FGF14), which is highly expressed in Purkinje cells (Shakkottai et al., 2009; Xiao et al., 2013). FGF14 interacts with the C-termini of voltage-gated Na channels to alter their trafficking and gating (Liu et al., 2001; Lou et al., 2005; Laezza et al., 2007; Ali et al., 2016; Pablo and Pitt, 2016; Di Re et al., 2017). Knockdown or deletion of FGF14 slows Purkinje cell spontaneous firing in vivo and decreases $Na_V1.6$ expression (Shakkottai et al., 2009; Xiao et al., 2013; Bosch et al., 2015; Pablo et al., 2016). Knockdown also stabilizes Na channel inactivation and reduces resurgent Na current in cultured Purkinje cells (Yan et al., 2014).

Here, recording Na currents of acutely isolated mouse Purkinje neurons, we find that knockout (KO) of $Na_V\beta4$ has no detectable effects on Purkinje Na current, but transient current is briefer and resurgent current is reduced in the absence of FGF14. We identify multiple factors that may contribute to the effects of FGF14. First, we find that the splice variant FGF14-1a contains a sequence even more effective at Na channel block and unblock than the β4 peptide. Second, FGF14 deletion favors nonconducting states in a manner that is relatively resistant to site-3 toxin destabilization of inactivation. Third, resurgent current in Purkinje cells is disproportionately carried by highly tetrodotoxin (TTX)-sensitive Na current, which is selectively affected in FGF14-KO cells. These results indicate that FGF14 likely modulates several transitions among open, blocked, and inactivated states, maintaining a high availability of Purkinje cell Na channels during firing.

Materials and methods

All experiments were performed in accordance with institutional guidelines and were approved by the Northwestern University Institutional Animal Care and Use Committee, protocol number IS00000242 (I.M. Raman).

Mouse strains

Generation of $Na_V\beta4$ mutant mice

A 129S7/SvEv BAC clone (bMQ377-C2) containing the *scn4b* genomic locus (encoding the $Na_V\beta4$ protein) was transferred to SW102 bacterial cells and modified via recombineering to generate targeting vectors (Warming et al., 2005).

Scn4b *conditional* (scn4b^{fl}) *mice*

A 671-bp region including *scn4b* exon IV was replaced in one round of recombineering with a targeting cassette containing a 28-bp random genotyping tag, loxP-flanked *scn4b* exon IV, and a SpeI-flanked kanamycin resistance gene, by means of 40-bp homology arms. Kanamycin-resistant BAC clones were screened by PCR, and the recombined interval was sequenced. A verified targeted clone was then used to isolate a targeting vector in a second round of recombineering via gap repair. pBluescript SK+ was amplified by PCR to contain two 40-bp gap repair homology arms to isolate a targeting vector that includes a 3.0-kb 5′ homology arm and a 4.4-kb 3′ homology arm. Ampicillin-resistant clones were verified by PCR and sequencing. The resulting targeting vector was digested with SpeI to remove the Kan cassette, which was replaced with FRT flanked neomycin resistance gene (FNF) as an Avr II fragment.

To generate constitutive *scn4b* KO animals, *scn4b*^{fl} mice were crossed with E2a-Cre mice *FVB/N-Tg(EIIa-cre)C5379Lmgd/J* (JAX stock #003314; Lakso et al., 1996). The resulting allele is missing exon IV, and potential splicing from exon III to exon V is predicted to produce an immediate truncation of the coding sequence at the exon junction.

Scn4b *peptide deletion* (scn4b$^{\Delta p}$) *mice*

A 671-bp region including *scn4b* exon IV was replaced in one round of recombineering with a targeting cassette containing a 28-bp random genotyping tag and a mutated *scn4b* exon IV, and an AscI flanked kanamycin resistance gene, by means of 40-bp homology arms. The sequence alteration at the 3′ end of exon IV removes the sequences encoding the peptide FILKKTR. Kanamycin-resistant BAC clones were screened by PCR, and the recombined interval was sequenced. A targeting vector was isolated by gap repair as described above, and ampicillin-resistant clones were verified by PCR and sequencing. The resulting targeting vector was digested with AscI to remove the Kan cassette, which was replaced with an AscI-flanked autoexcising loxP-flanked neomycin resistance gene (ACNF).

For both mutations, mismatches were introduced into the *scn4b* exon IV region based on *Mus spretus* sequence, to inhibit homologous recombination in ES cells within the desired insertion (e.g., between loxP sites). Targeting vectors were linearized with PmeI and electroporated into a 129/X1 ES cell line (PRX-129). Recombined clones were identified by long-range PCR (Skarnes et al., 2011) and injected into C57BL/6J blastocysts. Male chimeras were bred to C57BL/6J females, and F1 progeny were intercrossed. To remove the FNF selection cassette from *scn4b*^{fl} allele, F1 mice were crossed to ROSA-flpO mice *B6.129S4-Gt(ROSA)26Sor*$^{tm2(FLP^*)Sor}$*/J* (Jax #012930).

FGF14$^{-/-}$ *mice*

FGF14$^{-/-}$ mice, originally developed by Wang et al. (2002), were a gift from the laboratory of Jeanne Nerbonne (Washington University, St. Louis, MO). These mice contain a deletion of exons II and III of the *fgf14* gene, which encode the entire core region of the protein. In place of the deleted exons is an insertion of the gene encoding β-galactosidase, resulting in the expression of a fusion protein consisting of β-galactosidase and the

alternatively spliced N-terminus of FGF14-1a or 1b. Based on previous studies, it is likely that the function of FGF14 protein is greatly disrupted in these mice (Wang et al., 2002; Shakkottai et al., 2009; Bosch et al., 2015). FGF14 mutant mice were bred as heterozygotes, and homozygous littermates (+/+ and −/−) were used for recording. Both sexes of mice were used for experiments, and sex was recorded. Summary data for each sex in each dataset are reported.

Quantitative PCR

$Na_V\beta4$ mRNA expression in $Na_V\beta4^{-/-}$ and $Na_V\beta4^{\Delta p/\Delta p}$ mice was measured via qPCR, following MiQE (Minimum Information for Publication of Quantitative Real-Time PCR Experiments) guidelines (Bustin et al., 2009). Cerebella were dissected from homozygous mutant mice and WT littermates (P12–20), and RNA was extracted using RNeasy RNA isolation kit (Qiagen), followed by treatment with DNase. RNA quality was assessed (Bioanalyzer), and only samples with an RNA integrity number >9 were used for analysis. cDNA synthesis was performed with Superscript III reverse transcription (Invitrogen) on 300 ng RNA. qPCR was performed with three sets of intron-spanning primers covering various exons of the five-exon gene. Primer set A (exons I–II): forward 5′-GGAACCGAGGCAATACTCAG-3′, reverse 5′-TGAGCCGTTAATAGCGTAGATG-3′ (128 bp). Primer set B (exons IV–V): forward 5′-GGGTCATTGGACTTCTTGTTTG-3′, reverse 5′-TTCCCAGAGGAACTCACGAG-3′ (109 bp). Primer set C (exons III–V): forward 5′-CATCTTCCTCCAAGTGGTTG-3′, reverse 5′-AACTCACGAGACACTCCTTC-3′ (176 bp in WT). *Scn4b* gene expression was normalized to the reference gene, *Gusb*: forward 5′-GCTGATCACCCACACCAAAG-3′, reverse 5′-CAC AGATAACATCCACGTACG-3′ (107 bp). No-template controls were run for each primer set to test for contamination and primer dimers. pPCR was performed in 10-µl reactions contained 5 µl of iQ SYBR Green Supermix (Bio-Rad), 300 nM of each primer, and cDNA equivalent to 2 ng of RNA. Cycling was done using a Bio-Rad CFX384 Touch Real-Time PCR Detection System, cycling conditions: 95°C for 3 min, followed by 40 cycles of 95°C for 15 s and 59°C for 45 s. All reactions were run in triplicate, and no-template controls were run for every primer set. Melting curve analysis was run at the end to verify amplicon specificity.

Sequencing

A fragment of *scn4b* cDNA (from cerebellar RNA) spanning the mutation was amplified from mutant and WT littermates via PCR using the following primers: forward 5′-AGATACACCTGC TTCGTGAG-3′; reverse 5′-ACACTTTTGTGGGTGGCTTC-3′. Amplicons were gel extracted using Qiaquick Gel Extraction kit (Qiagen) and directly sequenced.

Cell isolation

Neurons were acutely dissociated from mice ages postnatal day (P) 12–20 for Purkinje cells and P8–15 for CA3 pyramidal cells, with procedures modified slightly from Raman and Bean (1997) and Raman et al. (1997) owing to changes in the available proteases. Mice were anesthetized with isoflurane, and sections of the cerebellar cortex or the whole hippocampus were dissected from the brain. Tissue was minced and incubated in preoxygenated dissociation solution (in mM: 82 Na_2SO_4, 30 K_2SO_4, 5 $MgCl_2$, 10 HEPES, 10 glucose, and 0.001% phenol red, pH 7.4, 300 mOsm) containing 2 mg/ml proteinase type XXIII (Sigma-Aldrich, P4032) at 30°C for 4 min (cerebellum) or 6 min (hippocampus). The tissue was then washed in oxygenated 30°C dissociation solution containing 1 mg/ml BSA (Sigma-Aldrich, A7030) and 1 mg/ml trypsin inhibitor (Sigma-Aldrich, T9253; pH 7.4 with NaOH) and microdissected into smaller pieces (cerebellum), or the CA3 region was dissected (hippocampus). The tissue was then triturated with a series of fire-polished Pasteur pipettes in 30°C oxygenated Tyrode's solution (in mM: 150 NaCl, 4 KCl, 2 $CaCl_2$, 2 $MgCl_2$, 10 HEPES, and 10 glucose, pH 7.4, 300 mOsm) and allowed to settle in the recording chamber for 30–60 min. Oxygenated 30°C Tyrode's solution was added to fill the chamber completely before recording and allowed to cool to room temperature. Recordings were made from cells ≤4 h after isolation.

Electrophysiological recording

All recordings were performed at room temperature (22–23°C). Dissociated cells were identified by morphology: Purkinje neurons were pear-shaped, while CA3 neurons were pyramidal. Recording pipettes pulled to 1.5–2.5-MΩ resistance were wrapped with parafilm to reduce capacitance and filled with internal solution (in mM: 108 $CsCH_3O_3S$, 9 NaCl, 4.5 TEACl, 1.8 $MgCl_2$, 4.5 EGTA, 9 HEPES, 4 MgATP, 14 Tris-creatine-PO_4, and 0.3 Tris-GTP, 300 mOsm with sucrose, pH 7.4 with CsOH). Voltage-clamped currents were recorded on an MultiClamp 700B amplifier and pClamp 10.3 (Molecular Devices), with series resistance compensated >70%.

After whole-cell access was achieved, cells were lifted from the bottom of the chamber and placed in front of gravity-driven quartz flow pipes containing either low-Na solution (in mM: 50 NaCl, 2 $BaCl_2$, 0.3 $CdCl_2$, 110 TEA-Cl, and 10 HEPES, pH 7.4, 300 mOsm) or high-Na solution (in mM: 100 NaCl, 2 $BaCl_2$, 0.3 $CdCl_2$, 5 TEA-Cl, and 10 HEPES, pH 7.4, 300 mOsm) to record Na currents. Recordings were repeated in the same solutions containing a saturating concentration (300 nM) of TTX to block voltage-gated Na channels (Moore and Narahashi, 1967). As noted, a subsaturating concentration of TTX (5 nM) was included in the control recording solution to reduce the magnitude of Na current and improve the quality of voltage clamp. For ATX experiments, 500 nM ATX was included in both recording solution and TTX solution. For CA3 recordings, the internal solution contained 200 or 400 µM peptide as indicated, and EGTA was reduced to 0.8 mM to minimize precipitation of peptides.

Peptides and drugs

Purkinje cell proteins containing sequences with homology to the β4 peptide were determined by searching RNA-seq data from the laboratory of Barbara Wold, California Institute of Technology, Pasadena, CA (https://www.encodeproject.org/experiments/ENCSR320PXZ), which provides RNA-seq data from a single Purkinje cell from a male mouse. Potential blocking peptides from these proteins were then designed to include 14–15 residues of the sequence that resembled the β4

peptide, along with residues expected to maximize likelihood of solubility. All peptides were synthesized by Life Technologies Pierce Custom Peptides. Multiple lots were used to verify replicability of results. Both ATX and TTX were purchased from Alomone Labs.

Data analysis, exclusion criteria, and statistics

Electrophysiological data were analyzed with Igor Pro version 7.0 (Wavemetrics). All Na currents were analyzed and displayed after records in 300 nM TTX were subtracted from records in control (0 or 5 nM TTX) solutions and therefore represent TTX-sensitive voltage gated Na current. The basic attributes of currents, such as presence or absence of resurgent currents, are reported for all cells in all experiments, but quantitative analyses are limited to cells with high-quality voltage clamp. The quality was considered to be high only if recordings fulfilled the following criteria: a) a gradual increase in peak current amplitude and decrease in time to peak, with progressively larger depolarizations between −60 and approximately −30 mV, without stepwise increases evident in the peak current–voltage relationship; and b) the absence of inflections generating a concave down region on the rising phase of Na currents, which was indicative of an escaping action potential.

Resurgent current (I_{rsg}) was measured either as absolute peak Na current evoked upon repolarization from +30 mV or as "relative resurgent current," i.e., peak resurgent current normalized to peak transient current (at 0 mV, except where stated to be −30 mV). Where only a single value for relative resurgent current is reported, the resurgent current at −30 mV was used in the normalization. Steady-state Na current (I_{ss}) was measured as the mean current in the last 10 ms of the depolarizing step after the decay of transient current and in the last 20 ms of the repolarizing step after the decay of resurgent current.

Decay phases of Na currents were fitted with single exponential decays or the sum of two exponential decays, each of the form $I_{Na} = A*\exp(-t/\tau) + I_{ss}$, where I_{Na} is peak Na current, A is amplitude, τ is the decay time constant, I_{ss} is the steady-state current, and t is time; where double exponential fits were used, the percentage contributed by the fast and slow components of decay were also estimated. For activation curves, peak transient currents evoked by step depolarizations from −90 mV were first converted to conductances by dividing by the driving force calculated from the predicted equilibrium potential. Activation curves of peak transient conductances were then fitted with a Boltzmann equation for activation of the form $G_{Na} = G_{max}/\{1 + \exp[-(V - V_{1/2})/k]\}$, where G_{Na} is conductance, G_{max} is the maximal conductance, V is the step potential, $V_{1/2}$ is the voltage at which half the conductance is activated, and k is the slope factor, indicating the depolarization necessary for an e-fold change in G_{Na}; in some cases, the data were first normalized by G_{max} and then fitted. Inactivation curves for transient current were computed by dividing the peak Na current elicited with a 10-ms step to 0 mV after 100-ms conditioning steps to a range of voltages by the peak transient current elicited by a step from −90 mV to 0 mV. The data were then fitted with a Boltzmann equation for inactivation of the form $I_{Na}/I_{max} = I_{ss} + (I_{Na} - I_{ss})/\{1 + \exp[(V - V_{1/2})/k]\}$, where I_{Na}/I_{max} is the normalized peak current, I_{ss} is the steady-state non-inactivated component of current, V is the step potential, $V_{1/2}$ is the voltage at which half the current is inactivated, and k is the slope factor. Data for each cell were fitted individually with activation and inactivation curves, and simulated curves with mean parameters are plotted.

In some traces, residual imperfectly subtracted capacitative transients were blanked for clarity. All data are reported as mean ± SEM. Statistical comparisons were made with Student's t test or one-way ANOVA with Tukey's post hoc, and P values are reported.

Results

Na currents in Na$_V$β4 mutant mice

Na$_V$β4 emerged as a good candidate for an Na channel blocker owing to its proximity to the channel and its proposed blocking sequence. However, several lines of evidence have suggested that Na$_V$β4 may not be the only factor contributing to resurgent Na current production. To test the extent to which Na$_V$β4 may be necessary for resurgent Na current, we developed a floxed Na$_V$β4 conditional KO (Na$_V$β4$^{fl/fl}$) mouse line, in which exon IV of the five-exon *scn4b* gene is flanked by loxP sites (Fig. 1 A). Exon IV encodes the single transmembrane domain of the protein, as well as the putative blocking peptide (Fig. 1 A, right). To generate a constitutive deletion allele, we crossed Na$_V$β4$^{fl/fl}$ mice with a germline Cre strain (E2a-Cre) to obtain F1 offspring with exon IV deleted. The allele was bred to homozygosity (Na$_V$β4$^{-/-}$), and the deletion was verified by PCR amplification and direct sequencing of tail DNA. *Scn4b* transcripts containing exon IV were detectable by quantitative PCR (qPCR) in WT controls but were undetectable in Na$_V$β4$^{-/-}$ mice, confirming deletion of the membrane-spanning domain and intracellular tail (Fig. 1, A [red arrows] and B). Although a transcript containing upstream exons (I to II) remained detectable in Na$_V$β4$^{-/-}$ mice, it was reduced by >60% compared with the WT transcript (Fig. 1, A [gray arrows] and B). To test whether the residual transcript spliced from exon III to V, we amplified cerebellar cDNA using intron-spanning primers (Fig. 1, A [black arrows] and B). Sequencing indeed revealed an abnormal splice, but it resulted in a coding sequence with a premature stop codon that would truncate the protein after exon III. Thus, despite the residual RNA-encoding upstream exons, the absence of the single transmembrane domain and the putative blocking sequence of Na$_V$β4 make it seem highly likely that functional protein was no longer expressed.

In addition, to control for effects resulting from loss of the whole Na$_V$β4 protein, we made a second, "peptide deletion" mouse (Na$_V$β4$^{\Delta p}$), in which seven key amino acids from the proposed blocking sequence were deleted (amino acid residues 189–195: FILKKTR; Fig. 1 A). We note that *scn4b* RNA levels from this allele were reduced by ∼20% compared with WT (Fig. 1 B). Sequencing of cerebellar cDNA from Na$_V$β4$^{\Delta p/\Delta p}$ mice confirmed that the desired sequence was deleted, so that any protein made lacked the putative blocking sequence of Na$_V$β4.

To test whether resurgent current was disrupted in either of these mice, we recorded voltage-clamped, TTX-sensitive Na currents from acutely dissociated Purkinje cells. In all electrophysiological

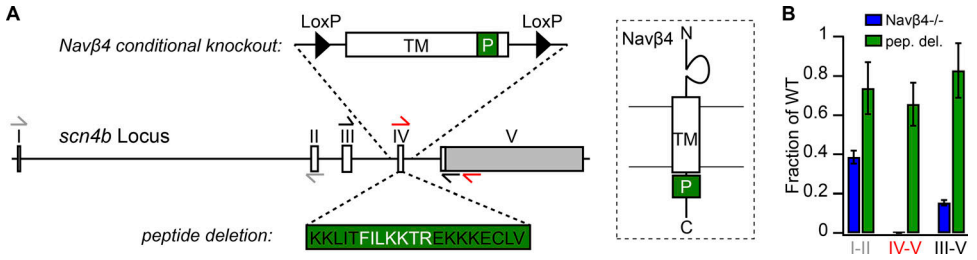

Figure 1. **Genetic strategy and validation of *scn4b* ($Na_V\beta4$) mutant mice. (A)** Left, Schematic illustrating the gene encoding $Na_V\beta4$ (*scn4b*), which contains five exons. Arrows represent PCR primers. The expanded region above shows exon IV, which includes the transmembrane (TM) domain and the β4 peptide (P) sequence, flanked by loxP sites. The expanded region below shows the β4 peptide sequence with amino acids deleted in the $Na_V\beta4^{\Delta p/\Delta p}$ (peptide deletion) mouse shown in white. Right, Schematic of the $Na_V\beta4$ protein in the membrane, showing location of regions targeted for deletion. **(B)** Fold change in mRNA expression (mean ± SEM) in $Na_V\beta4^{-/-}$ (blue) and peptide deletion (green) mice compared with WT littermates (n = 3 for each genotype), measured with qPCR primer set indicated by arrows in A (gray, spanning exons I and II; red, exons IV and V; black, exons III and V). Note, there was 0 mRNA expression in $Na_V\beta4^{-/-}$ mice with primers targeting exon IV (red arrows), confirming deletion of transmembrane and putative blocking regions.

experiments, sex was recorded. Because of the scarcity of mice of each genotype and the number of conditions being compared, we did not attempt to balance recordings from the sexes, and data from males and females are pooled, but all measurements segregated by sex are given in Tables 1, 2, 3, and 4, organized by figure number.

TTX-sensitive Na currents were recorded in eight cells from $Na_V\beta4^{+/+}$ WT mice and 25 cells from $Na_V\beta4^{-/-}$ KO littermates (P12–P18). In initial experiments, variable concentrations of subsaturating TTX (0, 5, or 10 nM) were included in the extracellular solution to reduce current magnitudes and improve voltage-clamp. In all WT cells, regardless of the concentration of

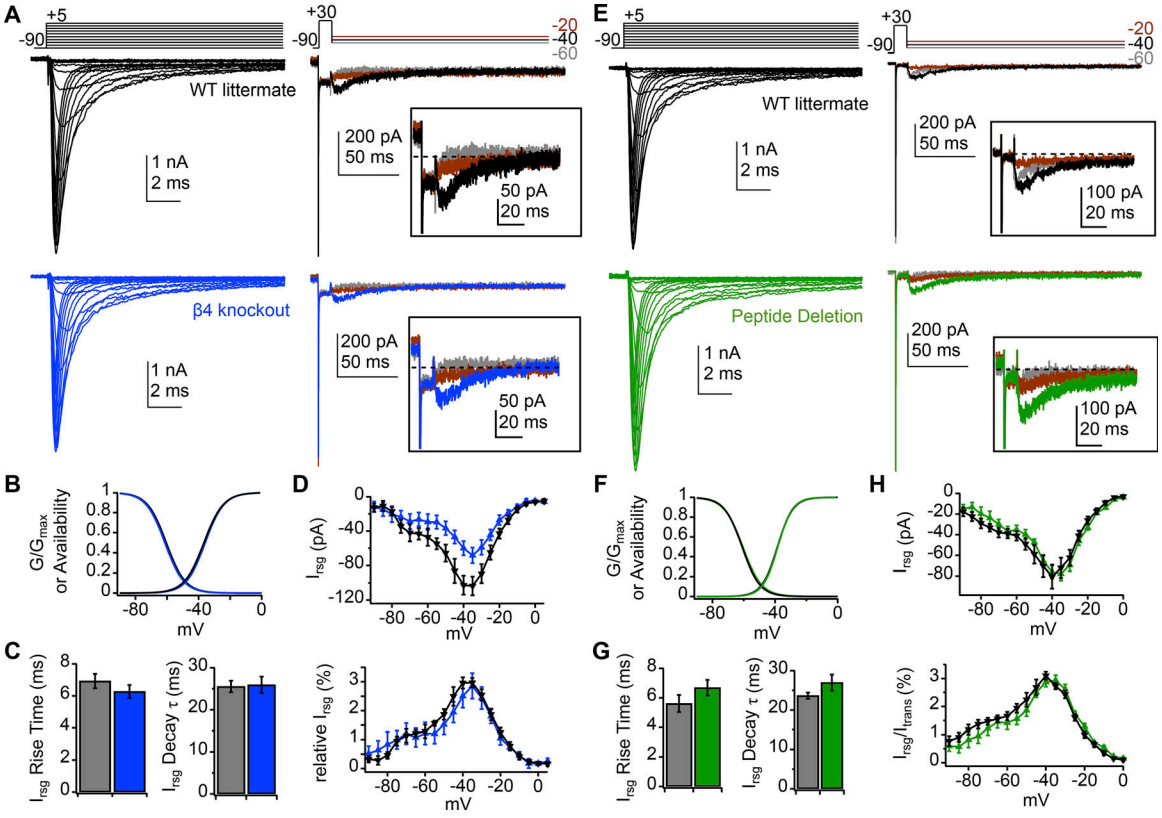

Figure 2. **Retention of normal transient and resurgent currents in $Na_V\beta4^{-/-}$ and peptide deletion Purkinje cells. (A)** Transient (left) and resurgent (right) Na current from a WT (black) and $Na_V\beta4^{-/-}$ (blue) isolated Purkinje cell (50 mM extracellular Na, 5 nM TTX). Inset, resurgent component at higher gain. **(B)** Activation and inactivation curves with mean parameters for WT (n = 6) and $Na_V\beta4^{-/-}$ (n = 8) Purkinje cells (values in text). **(C)** Rise time (left) and decay τ (right) of resurgent current at −30 mV for WT and $Na_V\beta4^{-/-}$ (values in text). **(D)** Peak absolute resurgent current versus voltage (top) and relative resurgent current versus voltage (bottom) for WT and $Na_V\beta4^{-/-}$. **(E–H)** Same as A–D but for cells from peptide deletion mice (green, n = 9) and WT littermates (black, n = 9). Resurgent current at −30 mV, −70.3 pA (WT), −92.1 pA (mutant); resurgent to transient ratios, 3.4% (WT), 3.2% (mutant). Data in C, D, G, and H are mean ± SEM.

Table 1. **Figure 2 electrophysiological measurements segregated by sex**

Measure	WT		$Na_V\beta4^{-/-}$		WT		$Na_V\beta4^{\Delta p/\Delta p}$	
	M (n = 4)	F (n = 2)	M (n = 2)	F (n = 6)	M (n = 6)	F (n = 3)	M (n = 6)	F (n = 3)
G_{max} (nS)	78.5 ± 8.1	107.2 ± 3	61.4 ± 0.18	61.5 ± 8.1	74.8 ± 8.5	44.7 ± 11	61.8 ± 5.8	76.1 ± 1.2
$V_{1/2}$ activation (mV)	−34 ± 2.6	−42 ± 6.3	−37.5 ± 3.5	−35.3 ± 0.6	−39.1 ± 3.2	−37.1 ± 1.9	−37.2 ± 1.3	−40.3 ± 0.6
k activation (mV)	5.97 ± 0.21	6.56 ± 1.53	6.13 ± 0.99	5.90 ± 0.39	4.65 ± 0.51	5.54 ± 0.53	4.59 ± 0.16	5.05 ± 0.58
$V_{1/2}$ inactivation (mV)	−59.7 ± 1.71	−62.3 ± 2.1	−58.1 ± 0.83	−62.5 ± 1.6	−61.3 ± 1.2	−60.6 ± 0.1	−60.6 ± 0.96	−60.7 ± 1.1
k inactivation (mV)	6.13 ± 0.26	5.72 ± 0.01	5.57 ± 0.05	6.12 ± 0.17	5.65 ± 0.21	5.62 ± 0.81	6.03 ± 0.22	6 ± 0.05
I_{rsg} rise (ms)	7.36 ± 0.55	6.07 ± 0.22	6.25 ± 1.36	6.29 ± 0.43	5.08 ± 0.37	6.67 ± 1.58	5.99 ± 0.43	8.09 ± 0.96
I_{rsg} decay τ (ms)	27.3 ± 2.1	26.5 ± 3.9	25.8 ± 0.95	27.6 ± 0.99	22.9 ± 0.53	23.4 ± 0.88	26.1 ± 3.6	28.5 ± 2
Relative rsg (%)	2.67 ± 0.28	2.3 ± 0.06	2.88 ± 0.39	2.28 ± 0.49	2.3 ± 0.19	2.69 ± 0.08	2.58 ± 0.26	2.7 ± 0.13

subsaturating TTX, transient currents at 0 mV exceeded 2 nA, and resurgent currents flowed upon repolarization to −30 mV after a 10-ms step to +30 mV. In all $Na_V\beta4^{-/-}$ cells, transient currents were large and resurgent currents were also evident, confirming that resurgent current can remain in Purkinje cells in the absence of functional $Na_V\beta4$ (Ransdell et al., 2017). Owing to high Na current densities and fast kinetics, however, the voltage-clamp of transient currents was not always ideal. We therefore quantified current magnitudes and kinetics only in the six WT and eight KO cells that satisfied criteria for well-clamped currents and good TTX subtractions (see Materials and methods); Na currents in all these cells were recorded in 5 nM TTX.

In both sets of cells, transient Na currents were robust, and resurgent Na currents were still present upon repolarization (Fig. 2 A). Loss of $Na_V\beta4$ did not affect the voltage dependence of activation and inactivation of the transient current relative to WT (Fig. 2 B; WT vs. $Na_V\beta4^{-/-}$, n = 6 and 8; $V_{1/2}$ activation: −36.6 ± 2.9 vs. −35.8 ± 0.81 mV, P = 0.8; $V_{1/2}$ inactivation: −60.6 ± 1.3 vs. −61.4 ± 1.3 mV, P = 0.7; k activation: 6.2 ± 0.4 vs. 6.0 ± 0.3 mV, P = 0.71; k inactivation: 6.0 ± 0.2 vs. 6.0 ± 0.1 mV, P = 0.97).

In the same cells, the kinetics of resurgent current measured at −30 mV were indistinguishable in WT and mutant mice (Fig. 2 C; WT vs. $Na_V\beta4^{-/-}$, rise time: 6.9 ± 0.4 vs. 6.3 ± 0.4 ms, P = 0.3; decay τ: 25.5 ± 1.4 vs. 25.9 ± 1.9 ms, P = 0.9). Plotting the current–voltage relation for peak resurgent Na currents values indicated that $Na_V\beta4^{-/-}$ cells in this dataset had smaller total resurgent current than their WT littermates (Fig. 2 D, top); however, the maximum Na conductance for $Na_V\beta4^{-/-}$ cells was also significantly smaller than for their WT littermates (WT vs. $Na_V\beta4^{-/-}$, G_{max}: 87 ± 8 vs. 61 ± 6 nS, P = 0.02). Although it initially seemed possible that this difference reflected mutation-induced changes in trafficking, a statistical difference was not evident in other subsets of cells tested (see below), consistent with previous observations that total current magnitudes vary widely across individual dissociated Purkinje cells (e.g., Raman et al., 1997). We therefore made all further comparisons using relative resurgent-to-transient current amplitudes. Indeed, when peak resurgent current values were normalized to the peak of the transient current measured at 0 mV (Fig. 2 D, bottom), the curves superimposed, indicating that the fraction of blocked Na channels was unchanged. The data therefore demonstrate that a protein other than $Na_V\beta4$ is fully capable of producing resurgent current in Purkinje cells that is indistinguishable from WT.

Recordings of Na currents in Purkinje cells from peptide deletion mice and their sibling controls gave largely similar results (Fig. 2 E). Again, the voltage dependence of activation and inactivation did not change (Fig. 2 F; WT vs. peptide deletion; n = 9, 9; $V_{1/2}$ activation: −38.4 ± 2.2 vs. −38.3 ± 1.0 mV, P = 0.9; $V_{1/2}$ inactivation: −61.1 ± 0.8 vs. −60.6 ± 0.7 mV, P = 0.7; k activation: 4.9 ± 0.4 vs. 4.7 ± 0.2 mV, P = 0.7; k inactivation: 5.6 ± 0.3 vs. 6.0 ± 0.1 mV, P = 0.2). The kinetics of resurgent current at −30 mV were also similar (Fig. 2 G; rise time: 5.6 ± 0.6 vs. 6.7 ± 0.5 ms, P = 0.2; decay τ: 23.7 ± 0.8 vs. 27 ± 2.0 ms, P = 0.2). Current–voltage relations indicated that the absolute resurgent current amplitude was the same in WT and mutant cells (Fig. 2 H, top), and the maximal transient Na conductance was also the same in both groups (G_{max}: 65 ± 8.1 vs. 67 ± 4.5 nS, P = 0.9), producing overlapping relative resurgent current–voltage curves (Fig. 2 H, bottom). The data provide further evidence that Purkinje cells must express other blocking factors, even when a blocking-peptide-free but otherwise intact $Na_V\beta4$ protein is present.

Identification of other proteins with putative blocking sequences

Previous studies of Na channel block by the 14-mer or 20-mer KKLITFILKKTREK[KKECLV], the β4 peptide, suggested that the residues necessary to produce resurgent current with kinetics similar to that seen in Purkinje cells were the phenylalanine (F6) and the positively charged residues that flank it (Grieco et al., 2005; Lewis and Raman, 2011). Therefore, to identify other potential blocking proteins, we searched open source RNA sequencing (RNA-seq) data from single Purkinje cells (see Materials and methods for link) for mRNA encoding proteins with the K2, F6, and K9 motif from the β4 peptide. This search yielded 164 proteins, of which $Na_V\beta4$ was the only protein with 100% identity to the β4 peptide. Based on a literature search, the list was narrowed down to nine proteins that were membrane bound or possibly cytosolic (i.e., not exclusively expressed in the nucleus), whose putative blocking sequence was likely to be intracellular, and that did not have a known function that

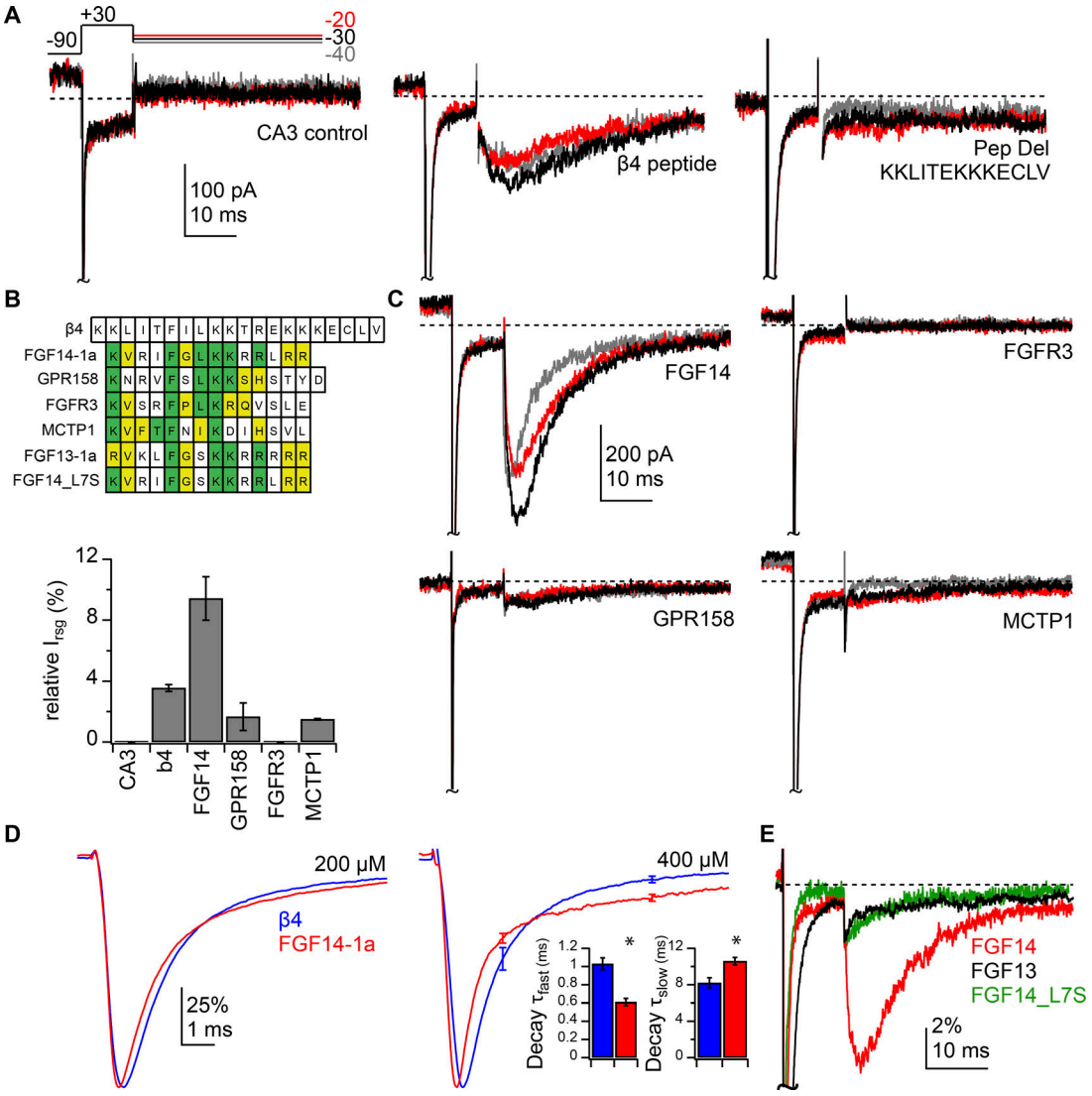

Figure 3. **Variable efficacy of open-channel block by peptides from Purkinje cell proteins expressing β4 peptide-like sequences. (A)** Na currents recorded in CA3 neurons without added intracellular peptides (left), with 200 μM β4 peptide (middle), and with 200 μM mutant β4 peptide mimicking the sequence in peptide-deletion mice (right). 50 mM extracellular Na, 0 TTX. Scale bars apply to all traces. **(B)** Top, Sequences of peptides tested aligned to the β4 peptide sequence. Green, conserved residues; yellow, conserved charge; white, nonconserved residues. Bottom, peak relative resurgent current for each peptide. **(C)** Na currents recorded with 200 μM intracellular FGF14-1a, GPR158, FGFR3, and MCTP1 peptides. Scale bars apply to all four traces. **(D)** Mean normalized transient current traces at −30 mV with 200 μM (left) or 400 μM (right) β4 (blue) or FGF14-1a (red) peptide. Scale bars apply to both traces. Inset, decay τ_{fast} and τ_{slow} for double exponential fits of transient current decay with 400 μM peptide. Data in B and D are mean ± SEM. *, P < 0.05. **(E)** Sample relative resurgent-like current traces with 200 μM FGF14-1a, FGF13-1a, and FGF14_L7S peptides.

apparently excluded it from being associated with Na channels. These nine proteins along with their putative blocking sequences are listed in Table 5. Of particular interest was FGF14-1a, since both the 1a and 1b isoforms of FGF14 are known to interact with the C-termini of Na channels and modulate their gating (Munoz-Sanjuan et al., 2000; Wang et al., 2000; Lou et al., 2005; Laezza et al., 2009; Pablo and Pitt, 2016; Di Re et al., 2017). Also, loss of FGF14 can slow firing rates of Purkinje cells as well as reduce resurgent current, although these effects have been largely ascribed to FGF14-1b (Shakkottai et al., 2009; Yan et al., 2014; Bosch et al., 2015).

To test whether any of these sequences were capable of producing resurgent current, we made use of synthetic peptides from the four proteins with sequences predicted to have the highest solubility based on hydrophilicity (FGF14-1a, GPR158, FGFR3, and MCTP1). Whole-cell recordings were made from acutely dissociated mouse CA3 hippocampal pyramidal neurons (WT and P8-P15), a cell type that completely lacks resurgent Na current until an effective open-channel–blocking peptide is added intracellularly (Raman and Bean, 1997; Grieco et al., 2005; Lewis and Raman, 2011). Consistent with previous work, CA3 cells did not produce resurgent Na current in the absence of added peptide (Fig. 3 A, left, $n = 4$), but with 200 μM β4 peptide in the internal solution, they generated a resurgent-like current upon repolarization to −30 mV that was ∼3% the amplitude of the transient current at 0 mV (Fig. 3, A [middle] and B [bottom],

Table 2. **Proteins expressed in Purkinje cells with sequence homology to the β4 peptide**

Gene name	Protein name	Blocking sequence
Scn4b	Sodium channel auxiliary subunit β4	KLITFILKK
FGF14-1a	Fibroblast growth factor homologous factor 14-1a	KVRIFGLKK
MCTP1	Multiple C2 domains, transmembrane 1	KVFTFNIKD
GPR158	Probable G protein–coupled receptor 158	KNRVFSLKK
FGFR3	Fibroblast growth factor receptor 3	KVSRFPLKR
GRM1	Glutamate receptor, metabotropic 1	KLLDFLIKS
ABCA5	ATP-binding cassette sub-family A member 5	KYISFCVKK
EDNRB	Endothelin receptor type B	KLVPFIQKA
ATRN	Attractin	KKVEFVLKQ
ANK2	Ankyrin-2	KMVNFLLKQ

n = 6). To confirm that the region of the peptide required for open-channel block corresponded to the deleted regions in the $Na_V\beta4$ mutant mice, we tested a peptide that mimicked the remaining coding region in the peptide deletion mice (KKLITEKKKECLV). This produced no resurgent-like current upon repolarization (Fig. 3 A, right, n = 8), indicating that in the peptide deletion mice, the remaining $Na_V\beta4$ protein was unlikely to be directly responsible for the resurgent current seen in Purkinje cells. When peptides with sequences shown in Fig. 3 B (top) were tested at 200 µM, the GPR158 and MCTP1 peptides produced small, fast resurgent-like currents (~2% of the transient), while the FGFR3 peptide produced no resurgent-like current upon repolarization (Fig. 3, B [bottom] and C, n = 5, 3, and 4).

In contrast, the peptide that mimicked FGF14-1a produced a large resurgent-like current that was ~9% of the amplitude of the transient current, i.e., threefold larger than the β4 peptide (Fig. 3, B [bottom] and C, n = 8). In addition, this resurgent-like Na current had faster kinetics than that seen with the β4 peptide (β4 vs. FGF14-1a, rise time: 7.5 ± 0.6 vs. 3.9 ± 0.21 ms, P = 0.001; decay τ: 23.0 ± 1.7 vs. 11 ± 0.7 ms, P = 0.003), suggesting that the FGF14-1a peptide bound to the Na channel with a lower affinity, unblocking the channel more quickly (Lewis and Raman, 2011).

The different affinities of the two peptides were also evident in the biexponential decay of transient current at −30 mV. The FGF14-1a peptide gave a briefer τ_{fast} and a longer τ_{slow} relative to the β4 peptide (Fig. 3 D, left; β4, n = 6; FGF14-1a, n = 8); when the experiment was repeated with 400 µM of either peptide, the difference in kinetics became more pronounced, making it more clearly attributable to the specific blocker (Fig. 3 D, right; β4, FGF14-1a, n = 4, 4; τ_{fast}: 1.0 ± 0.07 vs. 0.61 ± 0.04 ms, P = 0.003; τ_{slow}: 8.2 ± 0.6 vs. 11.0 ± 0.4 ms, P = 0.016; % fast: 88 ± 2 vs. 73 ± 4%, P = 0.016; transient current time to peak: 0.86 ± 0.09 vs. 0.62 ± 0.07 ms, P = 0.084). Previous work has provided evidence that the fast phase of decay at −30 mV reflects the block that occurs at all voltages, whereas the slow phase of decay reflects the expulsion of the blocker by permeating Na ions, allowing repeated reopening before the onset of classical inactivation (Raman and Bean, 2001; Aman and Raman, 2007, 2010). Here, the briefer τ_{fast} can be interpreted as the FGF14-1a peptide binding and blocking channels more readily than the β4 peptide, while the prolonged τ_{slow} with the FG14-1a peptide suggests multiple cycles of unbinding and binding, resulting in a longer decay phase and a larger persistent current later in the depolarizing step (Raman and Bean, 2001).

Like FGF14, other members of the fibroblast growth factor homologous factor family, i.e., FGF11, FGF12, and FGF13, are also intracellular modulators of voltage-gated Na channels (Pablo et al., 2016; Pablo and Pitt, 2016). We noted that the 1a isoform of FGF13 contains a sequence resembling the putative blocking sequence of FGF14-1a, including a phenylalanine flanked by positive residues, RVKLFGSKKRRRRR, raising the possibility that it, too, could block Na channels. We therefore tested the effects of introducing a peptide of this FGF13-1a sequence (200 µM) into the intracellular solution during recordings from CA3 cells. The FGF13-1a peptide produced only a very small, fast resurgent-like current upon repolarization (Fig. 3 E, n = 5), consistent with an extremely low-affinity binding to the pore (Lewis and Raman, 2011). Examination of the sequence suggested that the polar serine in position 7 of the FGF13-1a peptide might differ sufficiently from the nonpolar leucine in position 7 of the FGF14-1a peptide to hinder the ability of the FGF13-1a peptide to block Na channels. To test this possibility, we introduced a serine residue into the corresponding position of the FGF14-1a peptide: KVRIFGSKKRRLRR (FGF14 L7S). Indeed, FGF14 L7S no longer induced a large, slow resurgent-like current upon repolarization. Instead it generated small brief resurgent-like current, much like that of the FGF13-1a peptide in both amplitude and kinetics (Fig. 3 E, n = 3). This result demonstrates that the residues surrounding the phenylalanine can exert a significant effect on the affinity of blocker-like proteins.

Na currents in FGF14 mutant mice

As mentioned above, previous studies have demonstrated that short hairpin RNA (shRNA) knockdown of both the FGF14 1a and 1b isoforms in cultured Purkinje cells leads to a reduction in resurgent current, in a manner consistent with a stabilization of classical inactivation; the changes could be restored by expression of FGF14-1b alone (Yan et al., 2014). The putative blocking sequence, however, exists only in the alternatively spliced N-terminus of the 1a isoform, raising the possibility that the two isoforms together exert multiple effects on the channel. Therefore, to explore further the mechanisms by which FGF14 modulates resurgent current, we recorded TTX-sensitive Na currents from Purkinje cells of FGF14 KO ($FGF14^{-/-}$) mice, which lack both isoforms of the protein (Wang et al., 2002; see Materials and methods). Fig. 4 A shows example transient and resurgent current traces recorded in 5 nM TTX from $FGF14^{-/-}$ and WT littermates. The voltage dependence of transient Na current activation and inactivation were statistically unchanged in the KO mice (Fig. 4 B; WT vs. $FGF14^{-/-}$; n = 9, 9; $V_{1/2}$ activation: −38.0 ± 1.6 vs. −40.3 ± 2.1 mV, P = 0.5; $V_{1/2}$ inactivation: −59 ± 1.3 vs. −61.4 ± 1.3 mV, P = 0.2; k activation: 6.0 ± 0.7 vs. 5.2 ± 0.5 mV, P = 0.37; k inactivation: 5.8 ± 0.16 vs. 5.9 ± 0.1 mV, P = 0.8),

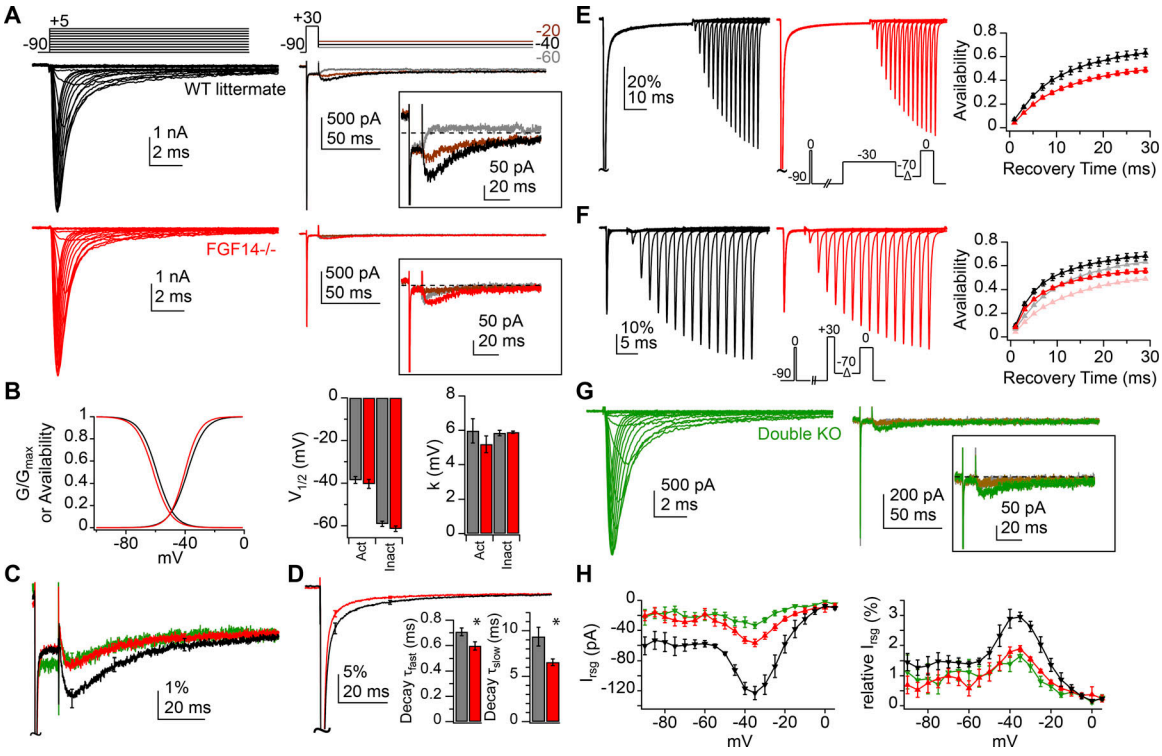

Figure 4. **Reduction of resurgent current and acceleration of transient current decay with deletion of FGF14 with and without $Na_V\beta4$. (A)** Transient (left) and resurgent (right) Na current from sample WT (black) and FGF14$^{-/-}$ (red) Purkinje cells (50 mM extracellular Na, 5 nM TTX). Insets, resurgent component at higher gain. **(B)** Left, activation and inactivation curves with mean parameters for WT (n = 9) and FGF14$^{-/-}$ (n = 9). Right, $V_{1/2}$ and k values for activation and inactivation (values in text). **(C)** Mean resurgent Na current normalized to the peak transient current at −30 mV for WT (black, n = 7), FGF14$^{-/-}$ (red, n = 7), and double KO (FGF14$^{-/-}$ and $Na_V\beta4^{-/-}$) cells (green, n = 8). Error bars show SEM at intervals. **(D)** Mean transient Na current normalized to peak transient current at −30 mV for WT (n = 7) and FGF14$^{-/-}$ (n = 7) cells. Insets, decay τ values from double exponential fit of transient current decay (values in text). *, P < 0.05. **(E)** Transient currents (left) in response to recovery voltage protocol (inset) for sample WT (black) and FGF14$^{-/-}$ (red) cells conditioned at −30 mV for 40 ms (in 0 TTX). Scale bars apply to both traces. Right, mean recovery curves for WT (n = 5) and FGF14$^{-/-}$ (n = 4) cells. **(F)** As in E, but for conditioning step to +30 mV for 5 ms (inset). Summary data from cells conditioned at −30 mV is plotted in light colors for comparison (right). **(G)** Transient (left) and resurgent (right) Na current in double KO cells (50 mM extracellular Na, 5 nM TTX). Inset, resurgent component at higher gain. **(H)** Peak absolute resurgent current versus voltage (left) and relative resurgent current versus voltage (right) for WT, FGF14$^{-/-}$, and double KO. Data in B, D, E, F, and H are mean ± SEM.

although both shifted slightly negative as in previous reports (Yan et al., 2014; Bosch et al., 2015). Absolute resurgent current amplitude in FGF14$^{-/-}$ neurons was reduced in amplitude relative to WT cells (Fig. 4 H, left). The maximum Na conductance was not significantly reduced in FGF14$^{-/-}$ cells (WT vs. FGF14$^{-/-}$; G_{max}: 88 ± 9.7 vs. 77.2 ± 8.4 nS, P = 0.4), so relative resurgent currents remained smaller in FGF14$^{-/-}$ cells (Fig. 4 H, right), indicating that the cycle of Na channel block and unblock was indeed altered in the absence of FGF14, although block was not abolished.

The residual resurgent current, however, retained kinetics that were indistinguishable from WT (Fig. 4 C; WT vs. FGF14$^{-/-}$, rise time at −30 mV: 8.0 ± 0.7 vs. 7.7 ± 0.9 ms, P = 0.8; decay τ at −30 mV: 26.8 ± 1.3 vs. 27.6 ± 2.9 ms, P = 0.8). These results suggest that the extent rather than the affinity of channel block is reduced in the absence of FGF14, which can happen if the onset of classical inactivation is increased (Khaliq et al., 2003; Grieco and Raman, 2004). Indeed, the transient current at −30 mV decayed more rapidly in FGF14$^{-/-}$ cells than in WT cells (Fig. 4 D; WT vs. FGF14$^{-/-}$, decay τ_{fast}: 0.7 ± 0.03 vs. 0.6 ± 0.03 ms, P = 0.02; decay τ_{slow}: 9.3 ± 1.0 vs. 6.6 ± 0.4 ms, P = 0.03; % fast: 90.5 ± 1.2 vs. 94 ± 0.6%, P = 0.02; I_{SS}: −18.5 ± 3.8 vs. −13.5 ± 5.1 pA, P = 0.4), consistent with a faster decay rate of the current without FGF14, as previously reported for cultured Purkinje cells (Yan et al., 2014).

Previous studies have shown that FGF14-1a expression in heterologous systems leads to a use-dependent cumulative "long-term" inactivation of Na channels and a slower recovery from inactivation (Laezza et al., 2009; Dover et al., 2010). The present results, in contrast, suggest that Na channels inactivated more stably when FGF14 was absent from Purkinje cells (Fig. 4, B and D). We therefore directly tested how recovery from inactivation was affected by deletion of FGF14. An initial reference step from −90 to 0 mV was applied to assess the maximal transient current amplitude. After a 200-ms interval, sufficient for full recovery, a conditioning step was applied either to −30 mV for 40 ms (to favor equilibration into inactivated states) or to +30 mV for 5 ms (to favor equilibration into blocked states; Fig. 4, E and F, WT, FGF14$^{-/-}$; n = 5 and 4; Raman and Bean, 2001; Aman and Raman, 2007). Channels then recovered at −70 mV for variable intervals before a test step to 0 mV was applied. The percentage recovery was calculated as the test current

Table 3. **Figure 4 electrophysiological measurements segregated by sex**

Measure	WT		FGF14$^{-/-}$		Double KO	
	M (n = 2)	F (n = 8)	M (n = 1)	F (n = 8)	M (n = 5)	F (n = 3)
G_{max} (nS)	46.5 ± 10.6	98.3 ± 8.5	98.9	74.5 ± 9	44.2 ± 4.4	65.1 ± 9.2
$V_{1/2}$ activation (mV)	−38.2 ± 3.7	−38.6 ± 1.9	−33	−41.2 ± 2.1	−34.9 ± 3.1	−35.1 ± 3.5
k activation (mV)	5.2 ± 1.9	6.16 ± 0.8	5.78	5.11 ± 0.55	6.54 ± 0.47	5.44 ± 0.38
$V_{1/2}$ inactivation (mV)	−60 ± 1.6	−58.9 ± 1.6	−56.2	−62 ± 1.24	−62.1 ± 0.77	−61.5 ± 1.2
k inactivation (mV)	5.92 ± 0.29	5.82 ± 0.2	5.85	5.9 ± 0.1	6.37 ± 0.32	5.99 ± 0.06
I_{rsg} rise (ms)	7.39 ± 1.5	8.11 ± 0.87	8.32	7.59 ± 1	5.08 ± 1.5	8.87 ± 0.62
I_{rsg} decay τ (ms)	28.2 ± 8	26.5 ± 0.72	14.4	29.2 ± 2.7	19.6 ± 3.5	27.8 ± 1.7
Relative rsg (%)	3.34 ± 0.77	2.63 ± 0.17	1.41	1.57 ± 0.07	1.37 ± 0.31	1.25 ± 0.26
I_{trans}decay τ_{fast} (ms)	0.75 ± 0.06	0.70 ± 0.04	0.69	0.59 ± 0.03	0.85 ± 0.15	1.02 ± 0.25
I_{trans}decay τ_{slow} (ms)	6.96 ± 1.4	9.95 ± 1.2	6.98	6.51 ± 0.41	7.05 ± 1.6	7.52 ± 0.74
τ recovery (−30 mV; ms)		10.5 ± 0.97		11.1 ± 0.55		
Maximum recovery (−30 mV; %)		67.3 ± 3.1		52.3 ± 2.1		
τ_{fast} recovery (+30 mV; ms)		2.16 ± 0.34		2.28 ± 0.3		
τ_{slow} recovery (+30 mV; ms)		12.1 ± 1.2		12.4 ± 1.5		
Maximum recovery (+30 mV; %)		72.3 ± 2.8		59.6 ± 3.0		

normalized to the reference current. At both voltages, the recovery rate was comparable in WT and mutants, but the extent of recovery was lower without FGF14 (conditioning at −30 mV; WT vs. FGF14$^{-/-}$, single exponential recovery τ, 10.5 ± 1 vs. 11.1 ± 0.6 ms, P = 0.6; maximum recovery, 67.3 ± 3.1 vs. 52.3 ± 2.1%, P = 0.006; conditioning at +30 mV, double exponential recovery τ_{fast}, 2.2 ± 0.3 vs. 2.3 ± 0.3 ms, P = 0.8; τ_{slow}, 12.1 ± 1.2 vs. 12.4 ± 1.5 ms, P = 0.9; maximum recovery, 72.3 ± 2.8 vs. 59.6 ± 3%, P = 0.02). These data suggest that the primary effect of FGF14 in Purkinje cells is to favor availability of Na channels rather than to induce their inactivation. They also provide further evidence that the functional properties of Na channels and their associated proteins depend on cellular context.

One explanation for the effect of FGF14 deletion on transient and resurgent current is that FGF14 normally increases resurgent current simply by slowing the onset of fast inactivation, thereby permitting more channels to be blocked. However, because the decay of the transient current reflects contributions of both classical inactivation and block (Raman and Bean, 2001; Aman and Raman, 2007, 2010), an additional, nonexclusive possibility is that Purkinje cells express multiple blocking proteins with different affinities for the channel. If FGF14-1a were a slower binding and/or lower-affinity blocker, then in its absence, the more rapid and/or higher-affinity binding of a remaining open-channel blocker, such as $Na_V\beta4$, might account for the faster transient decay and smaller resurgent current.

To examine this possibility, we crossed the $Na_V\beta4^{-/-}$ mice with FGF14$^{-/-}$ mice to create offspring that included mice with a double KO of both proteins. Resurgent current, however, was still present in Purkinje cells of double KO mice (Fig. 4 G) and, when normalized to transient amplitude, had kinetics and relative amplitude indistinguishable from that of FGF14$^{-/-}$ mice (Fig. 4, C and H, n = 8). Thus, despite the blocking peptides present in $Na_V\beta4$ and FGF14-1a, both of which are part of Purkinje Na channel complexes, Purkinje neurons retain the ability to generate resurgent current in the absence of both proteins.

Effects of a site-3 toxin on Na currents in FGF14 mutant mice

We reasoned that if the primary effect of FGF14 deletion is to accelerate fast inactivation, which in turn reduces open-channel block by the native blocking protein, the magnitude of resurgent current might be restored by slowing fast inactivation. We therefore interfered with the outward movement of the DIVS4 voltage sensor with the site-3 toxin anemone toxin II (ATX; Hanck and Sheets, 2007), which prolongs Na currents and increases resurgent current amplitudes, presumably by favoring block over inactivation (Bant et al., 2013; Lewis and Raman, 2013). These experiments were done in the absence of TTX. Fig. 5 A shows the mean transient and resurgent Na current traces at −30 mV with and without 500 nM ATX from Purkinje cells of FGF14$^{-/-}$ mice, double (FGF14$^{-/-}$ and $Na_V\beta4^{-/-}$) KO mice, and their WT littermates (FGF14$^{+/+}$ and either $Na_V\beta4^{+/+}$ or $Na_V\beta4^{+/-}$). In all three genotypes, ATX slowed decay of the transient current and increased the peak of the resurgent current. Even in the presence of ATX, however, FGF14$^{-/-}$ cells and double KO cells retained significantly faster transient decay times and smaller resurgent currents than WT cells (WT, FGF14$^{-/-}$, double KO; n = 7, 6, and 9; transient decay τ_{slow} in ATX: 22.6 ± 0.7, 18.1 ± 1.1, and 17.7 ± 0.4 ms; Tukey's WT vs. FGF14$^{-/-}$ P = 0.006, and vs. double KO, P < 0.001), indicating that slowing classical inactivation was not sufficient to negate the effect of FGF14 loss.

Plotting the peak current voltage curves for the transient current indicated that Na channels activated at more negative

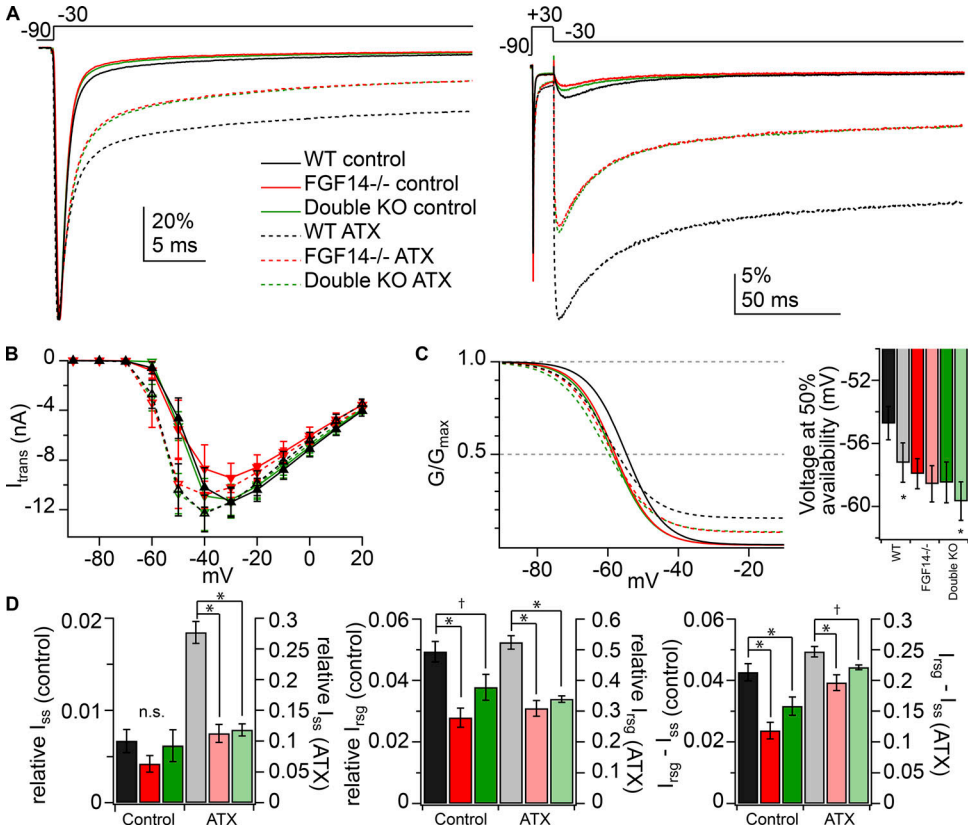

Figure 5. **Ability of ATX to increase resurgent and persistent Na currents without reversing effects of FGF14 deletion. (A)** Mean transient (left) and resurgent (right) Na current traces from WT (black, *n* = 7), FGF14$^{-/-}$ (red, *n* = 6), and double KO (green, *n* = 9) Purkinje cells in the presence (dotted lines) and absence (solid lines) of 500 nM ATX. Traces are normalized to the peak transient current at −30 mV (50 mM extracellular Na, 0 TTX). **(B)** Mean peak transient current–voltage relationships for WT, FGF14$^{-/-}$, and double KO cells with (dotted lines) and without (solid lines) ATX. Note left-shifted curves without large changes in peak current near 0 mV. **(C)** Left, Inactivation curves with mean parameters for WT, FGF14$^{-/-}$, and double KO cells with and without ATX. Right, Voltage at which channel availability is 50% for each condition (values in text). **(D)** Steady-state current (left), resurgent current (middle), and resurgent minus steady-state current (right), each normalized to transient current at 0 mV, for each condition. * P < 0.05; †, P < 0.1 (Tukey's post hoc). Data in B–D are mean ± SEM; n.s., not significant.

voltages in ATX in all three genotypes (Fig. 5 B). Despite the expected relief of fast inactivation and impeding of domain IV movement (Campos et al., 2008), ATX shifted the steady-state inactivation curve negatively in WT neurons, as previously noted (Fig. 5 C; Bant et al., 2013; Lewis and Raman, 2013). In contrast, in the mutant cells, in which inactivation curves were already negatively shifted relative to WT, this effect of ATX was reduced or absent (Fig. 5 C). Because the inactivation curves differed in the steady-state availability, which influences the estimation of the parameter $V_{1/2}$ with Boltzmann fits, we quantified the half-inactivation value simply as the voltage at which the test current at 0 mV fell to 50% of the peak availability (control vs. ATX, paired *t* tests: WT, −54.7 ± 1.0 vs. −57.2 ± 1.3 mV, P < 0.001; FGF14$^{-/-}$, −57.9 ± 1.0 vs. −58.6 ± 1.2 mV, P = 0.5; double KO, −58.5 ± 1.3 vs. −59.7 ± 1.3 mV, P = 0.02). Thus, although ATX is known to increase mean channel open time (Hanck and Sheets, 2007), it also apparently favors nonconducting states at more negative voltages, in a manner that is largely occluded by the absence of FGF14.

Application of ATX also differentially affected persistent current in each genotype. In control solutions, persistent current (normalized to peak transient current at 0 mV) was <1%, and its magnitude was comparable among genotypes (Fig. 5, A and D, left; WT, FGF14$^{-/-}$, double KO: 0.7 ± 0.1%, 0.4 ± 0.09%, and 0.6 ± 0.02%; Tukey's WT vs. FGF14$^{-/-}$ P = 0.5, and vs. double KO, P = 0.96). ATX greatly enlarged the persistent currents in all genotypes, but it did so to a much lesser extent in FGF14-lacking than in WT cells (Fig. 5, A and D, left; WT, FGF14$^{-/-}$, double KO: 27.7 ± 1.8%, 11.2 ± 1.5%, and 11.8 ± 1%; Tukey's WT vs. FGF14$^{-/-}$ P < 0.001, and vs. double KO, P < 0.001). These results are consistent with the foot of the availability curve, which is elevated more in WT cells than in FGF14-lacking cells.

Relative resurgent current tended to be smaller in the FGF14$^{-/-}$ and double KO cells than in WT cells in ATX-free, TTX-free solutions, as it was for recordings made in subsaturating TTX (Fig. 5, A and D, middle; WT, FGF14$^{-/-}$, double KO: 4.9 ± 0.3%, 2.8 ± 0.3%, and 3.8 ± 0.4%; Tukey's WT vs. FGF14$^{-/-}$ P = 0.004, and vs. double KO, P = 0.09). Like the persistent current, the peak current evoked upon repolarization was greatly increased by ATX in all genotypes, but to a lesser extent in the mutant cells. Consequently, the ATX-modulated resurgent current peak in FGF14-lacking cells was only ~60% of that in WT cells (Fig. 5 D, middle; WT, FGF14$^{-/-}$, double KO: 52.4 ± 2.2%, 30.9 ± 2.6%, and 34 ± 1%; Tukey's WT vs. FGF14$^{-/-}$ P < 0.001, and

Table 4. **Figure 5 electrophysiological measurements segregated by sex**

Measure	WT		FGF14$^{-/-}$		Double KO	
	M (n = 5)	F (n = 2)	M (n = 0)	F (n = 6)	M (n = 0)	F (n = 9)
I_{trans}decay τ_{slow} (ms) control	13.7 ± 1.5	16.4 ± 3.1		10.5 ± 0.41		11.3 ± 0.42
I_{trans}decay τ_{slow} (ms) ATX	22 ± 0.6	24.1 ± 1.7		18.1 ± 1.1		17.7 ± 0.44
V at 50% (mV) control	−55 ± 1.1	−54.1 ± 3.3		−57.9 ± 1		−58.5 ± 1.3
V at 50% (mV) ATX	−57.7 ± 1.1	−56.1 ± 4.3		−58.6 ± 1.2		−59.7 ± 1.2
Relative I_{ss} (%) control	0.8 ± 0.13	0.35 ± 0.1		0.42 ± 0.1		0.62 ± 0.17
Relative I_{ss} (%) ATX	25.9 ± 1.4	27.9 ± 4.4		11.2 ± 1.5		11.8 ± 1
Relative I_{rsg} (%) control	4.9 ± 0.48	5.03 ± 0.23		2.79 ± 0.31		3.78 ± 0.42
Relative I_{rsg} (%) ATX	49.6 ± 1.2	59.2 ± 4.7		30.9 ± 2.6		33.9 ± 1
I_{rsg}–I_{ss} (%) control	4.11 ± 0.37	4.68 ± 0.14		2.37 ± 0.27		3.16 ± 0.3
I_{rsg}–I_{ss} (%) ATX	23.8 ± 0.89	27 ± 0.3		19.7 ± 1.3		22.1 ± 0.38

vs. double KO, P < 0.001). Notably, however, the WT and FGF14-lacking resurgent currents seemed to run largely parallel to each other with no clear distinction in kinetics, as though the difference was a nearly constant value. Therefore, we subtracted the persistent current at the end of the voltage step from the resurgent current peak amplitude and compared the currents again. With persistent current removed, the difference between resurgent and steady-state current (I_{rsg} − I_{ss}) amplitude of FGF14$^{-/-}$ and double KO cells compared with WT was less pronounced, with the ATX-modulated persistent-subtracted resurgent current being 80–88% of the amplitude in the WT cells (Fig. 5 D, right, control solutions, WT, FGF14$^{-/-}$, double KO: 4.3 ± 0.3%, 2.4 ± 0.3%, and 3.2 ± 0.3%; Tukey's WT vs. FGF14$^{-/-}$ P = 0.001, and vs. double KO, P = 0.03; in ATX: 24.7 ± 0.9%, 19.6 ± 1.3%, and 22.1 ± 0.4%; Tukey's WT vs. FGF14$^{-/-}$ P = 0.002, and vs. double KO, P = 0.08). Thus, the dominant effect of ATX seems to be to increase persistent current, consistent with a prolongation of channel open time (Hanck and Sheets, 2007). Additionally, although the time course of current decay is slowed, ATX also left-shifts the macroscopic inactivation curve. These effects of ATX are at least partly occluded by loss of FGF14; conversely, the effects of FGF14 deletion cannot be reversed by interfering with deployment of the DIV voltage sensor.

Differential TTX sensitivity of transient and resurgent Na current

We noted that in the ATX-free control records made in the absence of TTX, the magnitude of relative resurgent current appeared to be greater than in the recordings made in subsaturating (5 nM) TTX, raising the possibility that low doses of TTX might preferentially block a subset of Na channel α subunits that produced the largest resurgent currents, e.g., $Na_V1.6$ (Raman et al., 1997). We therefore investigated the effects of subsaturating TTX on Na channel kinetics and resurgent current by making within-cell comparisons of Na currents recorded at 0 and 5 nM TTX in Purkinje cells of WT, $Na_V\beta4^{-/-}$, FGF14$^{-/-}$, and double KO cells (in all cases, recordings were repeated in 300 nM TTX for subtractions). These recordings were made in 100 mM extracellular Na to enlarge resurgent current preferentially (Afshari et al., 2004). Transient currents averaged across all cells during a step from −90 to −30 mV from cells of each genotype in 0 (solid line) and 5 nM (dashed line) TTX (Fig. 6 A, left) and mean current–voltage curves (Fig. 6 A, right) illustrated that, across voltages, 5 nM TTX reduced transient current for all genotypes to a comparable extent (percentage reduction of peak transient current at −30 mV in 5 nM TTX: WT, $Na_V\beta4^{-/-}$, FGF14$^{-/-}$, double KO; n = 9, 9, 9, and 8; 47 ± 4%, 44 ± 3%, 46 ± 3%, and 50 ± 4%; one-way ANOVA, P = 0.6). These results suggested that either the complement of α subunits expressed is relatively unchanged across genotypes or that all α subunits have identical TTX sensitivity.

Consistent with previous recordings, decay of the transient current was faster in FGF14$^{-/-}$ and double KO cells than in WT and $Na_V\beta4^{-/-}$ cells, in both the presence and absence of 5 nM TTX. Within genotypes, however, the transient current decay also changed in 5 nM TTX, so that the fast component was prolonged and the slow component was accelerated, consistent with a decrease of open-channel block (Fig. 6 B, Raman and Bean, 1997; 0 vs. 5 nM TTX paired t tests: transient current at −30 mV decay τ_{fast}: WT 0.6 ± 0.02 vs. 0.7 ± 0.04 ms, P = 0.003; $Na_V\beta4^{-/-}$ 0.6 ± 0.02 vs. 0.7 ± 0.03 ms, P < 0.001; FGF14$^{-/-}$ 0.5 ± 0.02 vs. 0.6 ± 0.04 ms, P = 0.05; double KO 0.5 ± 0.01 vs. 0.7 ± 0.06, P = 0.03; decay τ_{slow}: WT 16.7 ± 1.2 vs. 12.9 ± 0.8 ms, P = 0.006; $Na_V\beta4^{-/-}$ 19.3 ± 1.2 vs. 14.7 ± 0.9 ms, P < 0.001; FGF14$^{-/-}$ 14.9 ± 1.0 vs. 11.2 ± 1.3 ms, P < 0.001; double KO 14.1 ± 1.2 vs. 10.4 ± 1.1 ms, P < 0.001; % fast: WT 93.4 ± 0.5% vs. 94 ± 0.7%, P = 0.8; $Na_V\beta4^{-/-}$ 94.5 ± 0.2% vs. 94.6 ± 0.8%, P = 0.9; FGF14$^{-/-}$ 95 ± 0.4% vs. 95.3 ± 0.8%, P = 0.5; double KO 95 ± 0.5% vs. 94.7 ± 1.2%, P = 0.8). Consistent with previous studies linking the slow phase of decay to the unbinding of the blocker (Raman and Bean, 2001; Aman and Raman, 2007), the relative resurgent current amplitude was also reduced in all genotypes in the presence of 5 nM TTX (Fig. 6 C; 0 vs. 5 nM TTX, paired t tests, relative I_{rsg} at −30 mV: WT 6.1 ± 0.9% vs. 3.3 ± 0.2%, P = 0.02; $Na_V\beta4^{-/-}$ 5.5 ± 0.5% vs. 3.3 ± 0.2%, P < 0.001; FGF14$^{-/-}$ 4.1 ± 0.4% vs. 2.2 ± 0.1%, P < 0.001; double KO 4.1 ± 0.6% vs. 2.4 ± 0.2%, P = 0.002), and this result was replicated across voltages (Fig. 6 D). Indeed, when the relative resurgent current in 5 nM TTX was plotted against that

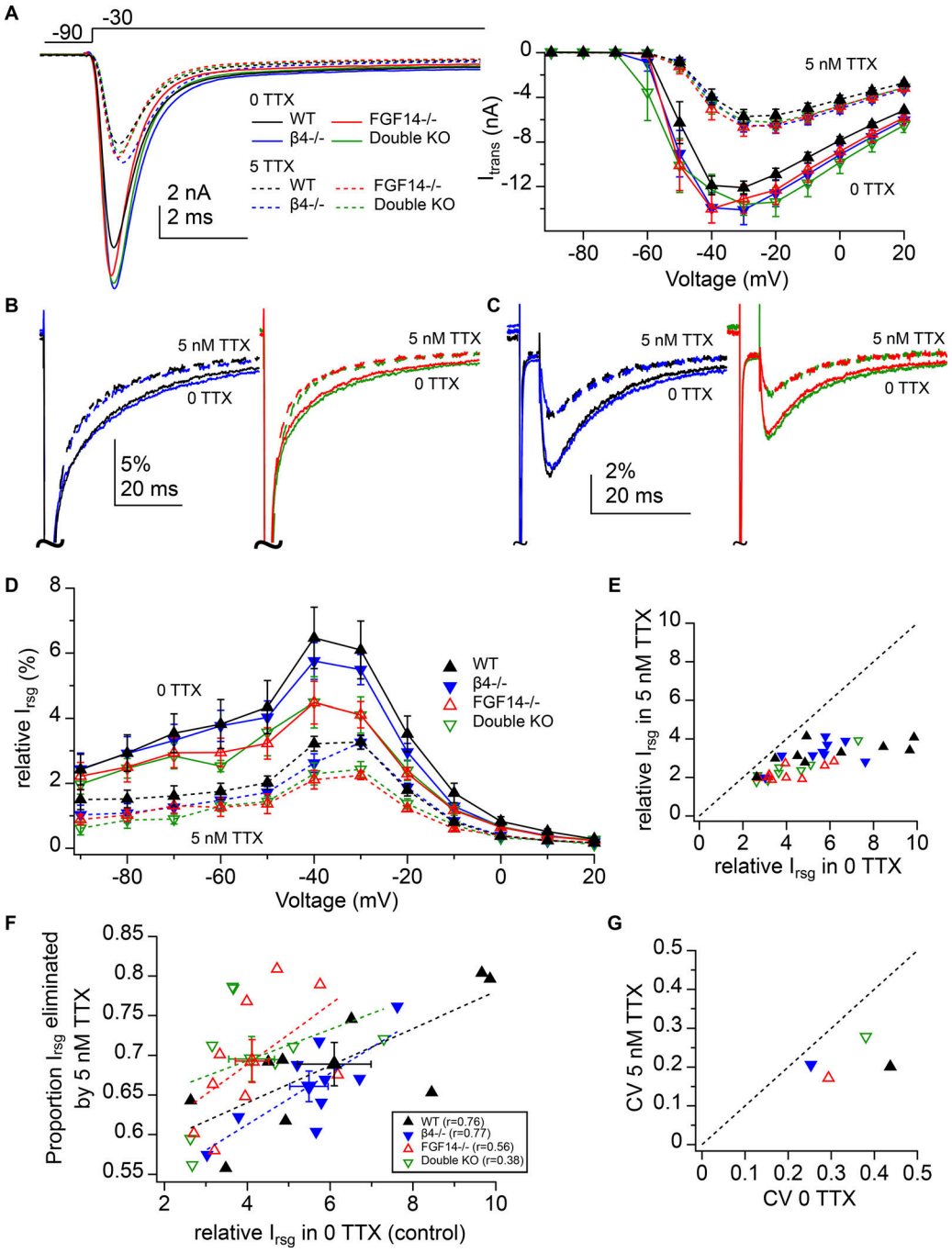

Figure 6. **Preferential contribution of highly TTX-sensitive Na channels to total and FGF14-modulated resurgent current. (A)** Left, Mean traces of transient current at −30 mV for WT (black, *n* = 9), $Na_V\beta4^{-/-}$ (blue, *n* = 9), $FGF14^{-/-}$ (red, *n* = 9), and double KO (green, *n* = 8) cells in the presence (dotted) and absence (solid) of 5 nM TTX (100 mM extracellular Na). Right, transient current–voltage relationships for each condition (mean ± SEM). **(B)** Mean transient currents shown in A, normalized to transient current peak at 0 mV. WT and $Na_V\beta4^{-/-}$ are overlaid (left), and $FGF14^{-/-}$ and double KO are overlaid (right) for clarity. **(C)** Mean resurgent current traces at −30 mV for each condition, normalized to transient current peak at 0 mV. **(D)** Relative resurgent current versus voltage for each condition (mean ± SEM). Note smaller relative resurgent current in subsaturating TTX. **(E)** Relative resurgent current peak in 5 nM versus 0 TTX for all cells. Dotted line indicates unity. **(F)** Proportion of the relative resurgent current at −30 mV blocked by 5 nM TTX versus relative resurgent current in 0 TTX from E. Symbols with error bars indicate mean ± SEM (values in text). Dotted lines, linear regression over points from each genotype. **(G)** Coefficient of variation of relative resurgent current for data from D in 5 nM TTX versus in 0 TTX (values in text). Dotted line indicates unity.

in 0 TTX for each cell, every point fell below the unity line (Fig. 6 E).

As is evident in Fig. 6 E, cells with larger resurgent current in control conditions tended to be more sensitive to 5 nM TTX. We therefore plotted the proportion of resurgent current eliminated by 5 nM TTX against the relative resurgent current in 0 TTX for every cell (Fig. 6 F). Linear regression over the points indicated that data were positively correlated in each of the four

Table 5. **Figure 6 electrophysiological measurements segregated by sex**

Measure	WT		$Na_V\beta4^{-/-}$		$FGF14^{-/-}$		Double KO	
	M (n = 2)	F (n = 7)	M (n = 5)	F (n = 4)	M (n = 6)	F (n = 3)	M (n = 4)	F (n = 4)
I_{trans} eliminated by TTX (%)	54 ± 0.51	44.9 ± 4.6	45.6 ± 3.7	42 ± 3.8	43.6 ± 3.6	51.3 ± 2.2	58.3 ± 5.1	42.1 ± 1.5
I_{trans}decay τ_{fast} (ms) control	0.62 ± 0.04	0.58 ± 0.02	0.58 ± 0.02	0.63 ± 0.03	0.53 ± 0.02	0.50 ± 0.04	0.54 ± 0.02	0.53 ± 0.02
I_{trans}decay τ_{fast} (ms) TTX	0.88 ± 0.06	0.67 ± 0.03	0.73 ± 0.05	0.77 ± 0.03	0.57 ± 0.02	0.70 ± 0.13	0.75 ± 0.11	0.61 ± 0.05
I_{trans}decay τ_{slow} (ms) control	12.8 ± 2.2	17.8 ± 1.1	18.9 ± 1.2	20 ± 2.6	15.8 ± 1.4	13.1 ± 0.4	15.4 ± 1.1	12.7 ± 2
I_{trans}decay τ_{slow} (ms) TTX	10.9 ± 3	13.4 ± 0.66	14.4 ± 0.96	15.2 ± 1.9	12.6 ± 1.7	8.45 ± 0.62	10.8 ± 1.5	9.94 ± 1.7
Fast control (%)	94 ± 0.1	93.3 ± 0.66	94.5 ± 0.31	94.5 ± 0.38	95.4 ± 0.47	94.2 ± 0.7	94.8 ± 0.93	95.1 ± 0.47
Fast TTX (%)	91.8 ± 0.65	94.7 ± 0.68	94.2 ± 1.2	95.2 ± 0.83	96.3 ± 0.64	93.3 ± 1.3	92.9 ± 1.8	96.4 ± 1.3
Relative I_{rsg} (%) Control	3.78 ± 1.2	6.76 ± 0.98	5.43 ± 0.48	5.57 ± 0.95	3.87 ± 0.51	4.6 ± 0.7	4.44 ± 0.96	3.77 ± 0.65
Relative I_{rsg} (%) TTX	3.08 ± 1.1	3.33 ± 0.16	3.53 ± 0.2	2.93 ± 0.36	2.28 ± 0.16	2.14 ± 0.24	2.63 ± 0.45	2.23 ± 0.19
Proportion I_{rsg} eliminated by TTX	0.63 ± 0.01	0.71 ± 0.03	0.64 ± 0.02	0.68 ± 0.04	0.66 ± 0.03	0.77 ± 0.03	0.75 ± 0.02	0.64 ± 0.04
CV control	0.43	0.38	0.20	0.34	0.32	0.26	0.43	0.35
CV TTX	0.49	0.13	0.13	0.25	0.17	0.19	0.34	0.17

genotypes, i.e., the larger the resurgent current in a particular cell, the more sensitive it was to low concentrations of TTX. Some differences emerged, however, between cells expressing and lacking FGF14. First, while 5 nM TTX blocked resurgent current equivalently across genotypes (proportion I_{rsg} eliminated: WT, $Na_V\beta4^{-/-}$, $FGF14^{-/-}$, double KO; 0.70 ± 0.03, 0.66 ± 0.02, 0.69 ± 0.03, and 0.70 ± 0.03; one-way ANOVA, P = 0.8), the data points for FGF-lacking cells were nevertheless relatively more clustered on the left side of the graph, although they did not fall below values in the control distribution. Second, the correlation coefficient (r) was lower in FGF14-lacking cells (WT r = 0.76, $Na_V\beta4^{-/-}$ r = 0.77, $FGF14^{-/-}$ r = 0.56, double KO r = 0.38), indicating that low-dose TTX sensitivity was less predictable from initial resurgent current magnitude in the absence of FGF14. These observations reinforce the idea that FGF14-lacking cells had smaller resurgent current amplitudes in control conditions but that the total complement of Na channel α subunits is similar across genotypes. In other words, the compression of data points suggests that the α subunits that produced more resurgent current in WT cells made relatively smaller resurgent currents without FGF14, while α subunits that made less resurgent current in WT cells did not change appreciably. In addition, low-dose TTX blockade reduced the variance of the relative resurgent current in all genotypes, as was evident by plotting the coefficient of variation (CV; the standard deviation divided by the mean; Fig. 6 G). For all four genotypes, the CV fell below the unity line (WT 0.44 vs. 0.2; $Na_V\beta4^{-/-}$ 0.25 vs. 0.21; $FGF14^{-/-}$ 0.29 vs. 0.17; and double KO 0.38 vs. 0.28), suggesting that α subunits that make relatively large resurgent currents are relatively selectively blocked.

Together, the data are consistent with the idea that Purkinje cells normally express multiple channels that differ in their ability to generate resurgent Na current, e.g., $Na_V1.6$, which is likely to be more effective, and $Na_V1.1$, which is likely less so (Raman et al., 1997; Grieco and Raman, 2004; Kalume et al., 2007). The present data further suggest that these channels have a differential sensitivity to TTX, as has been reported for expressed Na channels (Clare et al., 2000; Rosker et al., 2007; Lee and Ruben, 2008). Deletion of FGF14 appears to selectively reduce resurgent current flowing through Na channels with a higher sensitivity to TTX than other α subunits in Purkinje cells.

Discussion

The present results demonstrate that cerebellar Purkinje cells in 2–3-wk-old mice generate normal transient, persistent, and resurgent currents even when the gene encoding the $Na_V\beta4$ subunit is deleted, or when the residues in the cytoplasmic tail corresponding to the open-channel blocking β4 peptide are absent, indicating that alternative blocking proteins must exist. We find that Purkinje cells express other Na channel–associated proteins with open-channel blocker-like sequences, including FGF14-1a. A peptide fragment from FGF14-1a reversibly blocks Na channels in neurons lacking native open-channel blockers, generating larger resurgent-like currents than does the β4 peptide. As reported previously, Purkinje cells lacking FGF14 have more rapidly decaying transient currents and smaller resurgent currents than WT cells (Yan et al., 2014); KO of $Na_V\beta4$ in addition to FGF14 does not further alter Na currents. The observation that double KOs retain resurgent current rules out the possibility that these two subunits are the sole open channel blockers in Purkinje cells, despite the fact that they are both Na channel–associated subunits with domains capable of mimicking resurgent current that are highly expressed in Purkinje cells. Regarding the mechanism of action of FGF14, in both WT and FGF14-lacking cells, the site-3 toxin ATX prolongs transient currents and enlarges both resurgent and persistent currents, consistent with a slowed onset of fast inactivation and increased channel open time, but is not sufficient to reverse the effects of the loss of FGF14. In FGF14 mutants, the stabilization of nonconducting states, which may include blocked as well as inactivated states, appeared strongest in the subset of Na channels

that were most sensitive to low concentrations of TTX, which seem likely to correspond to $Na_V1.6$ subunits.

Evaluating $Na_V\beta4$ as an open-channel blocking protein

Considerable evidence supports the idea that the biophysical mechanism of resurgent Na current is a voltage-dependent open-channel block of the pore-forming subunit by an endogenous blocking protein (Raman and Bean, 2001; Grieco et al., 2002; Afshari et al., 2004; Grieco and Raman, 2004; Aman and Raman, 2010), but the identity of the blocking protein has remained elusive. So far, the most likely candidate has been $Na_V\beta4$. The original hypothesis was based on the ability of the β4 peptide to reconstitute resurgent current with the appropriate kinetics in Purkinje cell patches from which block had been removed and generate resurgent-like current in cells lacking a native blocker (Grieco et al., 2005). Additionally, the subunit was known to associate with Na channel α subunits (Yu et al., 2003), tended to be highly expressed in cells with resurgent current, and was often localized with $Na_V1.6$, an α subunit repeatedly implicated in generating resurgent current (Raman et al., 1997; Lewis and Raman, 2014). It has been clear, however, that $Na_V\beta4$ expression alone is insufficient to produce open-channel block of Na channels: resurgent current cannot be reconstituted by heterologous expression of $Na_V\beta4$ with pore-forming subunits (Chen et al., 2008; Aman et al., 2009; Theile et al., 2011), suggesting that other proteins or modifications might be necessary for $Na_V\beta4$ to produce resurgent current, and/or that other proteins with $Na_V\beta4$-like sequences instead act as Na channel blockers. Indeed, resurgent current can be generated by several variations in the β4 peptide sequence, making the idea of a family of blocking proteins seem plausible (Lewis and Raman, 2011).

Given the strong expression of $Na_V\beta4$ in Purkinje cells (Yu et al., 2003; Buffington and Rasband, 2013), it is nevertheless striking that isolated Purkinje cell bodies from *scn4b* deletion mice retain Na currents that are indistinguishable from controls. Evidence that the genetic manipulation was successful came from measurements and sequencing of mRNA. Moreover, Na currents indistinguishable from control were recorded from the peptide deletion, in which the $Na_V\beta4$ mutant protein is most likely still expressed, although its trafficking is uncertain. Because genetic changes in both mice were constitutive (present embryonically), however, it remains ambiguous whether $Na_V\beta4$ normally plays a role in somatic Purkinje cell currents that was obscured by compensatory activity of other proteins or expression of other genes. Indeed, regulation of gene expression in response to changes in neuronal activity and in response to genetic mutations has been widely reported (Turrigiano, 2008; El-Brolosy and Stainier, 2017; Yap and Greenberg, 2018). Nevertheless, the near-perfect match between currents in the presence and absence of the $Na_V\beta4$ blocking sequence, relative to both WT and the FGF14 KO, makes this idea seem somewhat implausible.

An alternative possibility is that $Na_V\beta4$ works in concert with one or more other blocking proteins that together produce resurgent current in WT Purkinje cells. If so, the other blocker is not limited to FGF14-1a, given the persistence of resurgent current in the double KO mice. Yet another possibility is that $Na_V\beta4$ is not responsible under any circumstances for producing resurgent current. Direct evidence to the contrary, however, comes from experiments showing that resurgent currents were reduced or abolished with shRNA knockdown of $Na_V\beta4$ in cerebellar granule cells, where it could be reconstituted with the β4 peptide (Bant and Raman, 2010), genetic deletion of *scn4b* in medium spiny striatal neurons (Miyazaki et al., 2014), or shRNA knockdown in DRG cells (Xie et al., 2016); conversely, $Na_V\beta4$ overexpression increased resurgent currents in DRG neurons (Barbosa et al., 2015). It seems more likely, therefore, that different neurons have distinct blocking proteins. Moreover, since granule cells and striatal cells have unmyelinated axons with high $Na_V\beta4$ expression in axons, and studies of the calyx of Held nerve terminal also provide good evidence for $Na_V\beta4$-dependent resurgent current (Kim et al., 2010; Berret et al., 2016), it is possible that $Na_V\beta4$ effects may be localized to regions other than the somata studied here, especially given evidence of high axonal expression of $Na_V\beta4$ in Purkinje cells (Buffington and Rasband, 2013). Thus, $Na_V\beta4$ may do little to modulate currents in WT Purkinje cell bodies. Notably, however, the present results differ from those reported by Ransdell et al. (2017), in which $Na_V\beta4$ was deleted using a different genetic approach and relative resurgent current was decreased but not eliminated. This discrepancy may be due to distinct compensatory mechanisms following the deletion of the protein using different approaches, or to different experimental conditions. Nevertheless, both sets of results suggest that Purkinje resurgent current can arise from mechanisms other than block by $Na_V\beta4$.

FGF14 and modulation of Purkinje cell Na currents

Based on identification of key residues involved in generating resurgent-like current by peptides (Lewis and Raman, 2011), we found naturally occurring sequences in proteins expressed by Purkinje cells matching those predicted for a blocking protein. Most strikingly, the sequence from FGF14-1a generated resurgent-like currents even larger than those produced by the β4 peptide. However, not all peptide fragments that resemble the β4 peptide sequence can act as open-channel blockers. An analogous sequence in FGF13-1a was unable to do so; this difference was likely due to one amino acid, and peptides from Purkinje cell proteins GPR158, FGFR3, and MCTP1 were relatively ineffective. These results indicate that the sequence is not so promiscuous that any protein with an aromatic ring flanked by positive charges can produce resurgent-like current.

The molecular characteristics for FGF14-1a make it a plausible candidate for an open-channel blocker. Intracellular FGF proteins are composed of a core region and alternatively spliced N-termini, and FGF14 has two distinct isoforms: 1a and 1b (Munoz-Sanjuan et al., 2000; Wang et al., 2000). The putative blocking sequence of FGF14 is located on the N-terminus of FGF14-1a but not 1b. The core region of the FGF14 protein interacts with the Na channel C-terminus (Liu et al., 2001; Laezza et al., 2009; Ali et al., 2016; Di Re et al., 2017), which could place the N-terminal tail of FGF14-1a close to the internal mouth of the pore. This position appears ideal for the putative blocking sequence to enter and bind to a pore-blocking site; indeed, when

chimeras with the β4 peptide at the end of FGF13-1a were heterologously expressed with $Na_V1.5$ subunits, tiny but detectable resurgent currents were generated (Barbosa et al., 2017). In addition, phosphorylation by casein kinase II is required for FGF14 to interact with the Na channel (Hsu et al., 2016), consistent with observations that phosphorylation is required for expression of resurgent current (Grieco et al., 2002). Together, these attributes suggest a means by which cells expressing the 1a isoform might produce resurgent current, while cells expressing FGF14-1b might relieve inactivation, thus modulating resurgent current if it is present, but not directly blocking the pore (Yan et al., 2014).

The FGF14-1a peptide bound Na channels with an apparently lower affinity than the β4 peptide, since resurgent current peaked earlier and the transient current had a slower second component of decay, indicative of the blocker flickering in and out of the channel more readily before inactivation (Raman and Bean, 2001; Aman and Raman, 2007, 2010; Lewis and Raman, 2011). One interpretation of the smaller relative resurgent current amplitudes and faster transient current decay in $FGF14^{-/-}$ Purkinje cells, therefore, is that FGF14-1a is indeed a natural blocker, and, when lost, a residual blocking particle binds the Na channel quickly with a higher affinity and is less readily expelled from the pore. Although the rise time of resurgent current is not detectably slowed in the absence of FGF14, the peaks might be truncated as a consequence of fast-inactivation-dependent current decay.

An alternative, though not mutually exclusive, interpretation is that loss of FGF14 simply led to an acceleration and stabilization of classical fast inactivation of Purkinje Na channels. Such an outcome could arise in two ways. Either FGF14 deletion could favor inactivation of existing channels and thereby reduce the probability of open-channel block by an unaffected blocker, or it could alter trafficking, thereby decreasing the expression of subunits that are readily susceptible to open-channel block. Regarding the former possibility, in $FGF14^{-/-}$ cultured Purkinje cells, which have reduced resurgent current, reexpression of FGF14-1b alone is sufficient to restore resurgent current amplitudes as well as transient current decay kinetics almost to control values (Yan et al., 2014). In the present experiments, however, application of ATX, which slows deployment of the domain IV voltage sensor (Hanck and Sheets, 2007), and which therefore might be expected to overcome effects solely due to a more rapid onset of fast inactivation, was insufficient to restore resurgent current to fully WT amplitudes. This observation could be consistent with a blocking effect of FGF14-1a. ATX and FGF14, however, interact with distinct sites on the Na channel. It is therefore possible that their effects are additive, such that ATX-mediated delay of domain IV movement is enhanced by the interference of FGF14 with the C-terminus. When FGF14 is deleted, therefore, the delay of inactivation induced by ATX may be reduced.

Regarding the latter possibility, of changing the complement of expressed α subunits, loss or mutation of FGF14 can indeed decrease of $Na_V1.6$ surface expression in the cell body and axon (Shakkottai et al., 2009; Xiao et al., 2013). Because most resurgent current in Purkinje cells is carried by $Na_V1.6$ subunits (Raman et al., 1997; Khaliq et al., 2003; Levin et al., 2006; Aman and Raman, 2007), resurgent current could be reduced in $FGF14^{-/-}$ Purkinje cells owing in part to preferential loss of $Na_V1.6$ surface expression. Thus, although FGF14-1a emerges as an appealing alternative candidate as an open-channel blocker, the extent to which it normally contributes to resurgent current in Purkinje cells remains ambiguous.

An additional caveat is that the $FGF14^{-/-}$ mouse used here is not a complete KO of FGF14 (Wang et al., 2002). Instead, exons encoding the core region of the protein were deleted and replaced by a sequence that encodes β-galactosidase. Exons encoding the alternatively spliced N-termini of FGF14-1a and -1b remain intact, resulting in expression of a protein containing the N-terminus fused to β-galactosidase. Because the putative blocking sequence is located on the N-terminus of FGF14-1a, this sequence is still present in these mice, and the fusion protein is in fact trafficked to axons (Wang et al., 2002). Normally, however, FGF14 interacts with the Na channel via its core region (Lou et al., 2005; Laezza et al., 2007; Goetz et al., 2009; Ali et al., 2014, 2016; Hsu et al., 2016), and Na currents in this mutant are indeed modulated differently from those in WT mice, suggesting a disruption in the FGF14-Na_V complex (Bosch et al., 2015). Therefore, even if the blocking sequence is present in the cell, the localization of the protein relative to the Na channel is probably not the same as with the native protein. Nevertheless, residual action of the mutant protein cannot be excluded.

TTX sensitivity

Relative resurgent current amplitudes were reduced when subsaturating concentrations of TTX were applied to the Purkinje cells. Comparisons of TTX sensitivity of different α subunits vary, possibly depending on expression system, but $Na_V1.6$ has been reported to have a slightly higher sensitivity to low concentrations of TTX than $Na_V1.1$ or $Na_V1.2$ (Smith et al., 1998; Clare et al., 2000; Rosker et al., 2007; Lee and Ruben, 2008); at the developmental stages of the present study, $Na_V1.1$, $Na_V1.2$, and $Na_V1.6$ are the most commonly expressed Na channel types in Purkinje cells (Schaller and Caldwell, 2003). Since Nav1.6 carries most of the resurgent current in Purkinje cells (Raman et al., 1997; Levin et al., 2006; Aman and Raman, 2007), a higher TTX sensitivity of Purkinje $Na_V1.6$ channels could account for the present observation that low (5 nM) TTX blocked a disproportionate amount of resurgent current. This idea is further supported by the observation that the CV of relative resurgent current amplitude decreases in 5 nM TTX, suggesting that the variety of channel types producing resurgent current is reduced by the differential block of Nav1.6 channels.

Alternative mechanisms for resurgent current

A possibility worth reconsidering is that Na channels produce resurgent current through a process entirely separate from open-channel block. If channels recover from fast inactivation through open states before deactivating, then upon repolarization from positive potentials, a gradually rising and decaying inward resurgent-like current would be produced; such current can be induced by toxins that favor outward positions of voltage sensors required for channel activation (Schiavon et al., 2006).

In normal channels, however, such a scenario would require recovery from fast inactivation at moderately negative potentials (near −30 mV) on the same time scale as the rise of resurgent current (near 5 ms). Such rapid recovery seems unlikely, since Purkinje Na channels take >10 ms to recover from fast inactivation even at potentials as negative as −90 mV (Aman and Raman, 2007), and recovery through open states from inactivation does not seem common in neurons even when it has been looked for carefully (Kuo and Bean, 1994).

Moreover, evidence for pore block comes from the observations that the magnitude of resurgent current is disproportionately sensitive to the extracellular concentration of Na^+ ions and directly proportional to the driving force on Na^+, to the point that resurgent current does not flow in the outward direction (Afshari et al., 2004; Aman and Raman, 2010). Thus, inwardly permeating Na ions are required for the recovery from the nonconducting state that channels enter upon depolarization, consistent with displacement of an open-channel blocker (Tang et al., 1996). In contrast, Na channel fast inactivation involves both activation of the DIVS4 voltage sensor and binding of the intracellular DIII-DIV linker to a binding site on the channel (West et al., 1992; Eaholtz et al., 1994; Yang and Horn, 1995; Kühn and Greeff, 1999; Capes et al., 2013; Ahern et al., 2016). While mutagenesis studies suggest that sites in the pore influence the receptor for the DIII-DIV linker (McPhee et al., 1994; Wang et al., 2003), recent structural evidence from cryo-EM studies shows that the linker binds outside the pore to a region involving the C-terminal domain of the channel, thus acting as an allosteric modulator that closes the intracellular helical bundle, leading to channel closure (Yan et al., 2017; Pan et al., 2018; Shen et al., 2019). This observation may help account for the role of the C-terminus in channel inactivation (Motoike et al., 2004). In addition, given that FGF14 binds to the C-terminus of the Na channel, it could delay binding of the DIII-DIV linker to its binding site, resulting in slower inactivation suitable to facilitate open-channel block by whichever native proteins are capable of reversible binding in the permeation pathway and thereby producing resurgent Na current.

Acknowledgments

José D. Faraldo-Gómez served as editor.

We are grateful to Sarah Kaye and Hardik Patel (Northwestern University) for technical assistance with qPCR and generation of mice, Dr. Jeanne Nerbonne (Washington University) for the gift of FGF14 mutant mice, and Dr. William Kath (Northwestern University) for help with RNA-seq. We thank Lynn Doglio and the Transgenesis and Targeted Mutagenesis Laboratory at Northwestern University for production of gene-targeted mice. Sequencing was done in the Northwestern University Sequencing (NUSeq) Core.

H.V. White was supported by National Institutes of Health T32-NS041234 and F31-NS108444. Research was supported by National Institutes of Health R37-NS39395 (I.M. Raman) and Bill and Gayle Cook Chair funds (I.M. Raman).

The authors declare no competing financial interests.

Author contributions: Experimental design of mutant mice, T.C. Bozza and I.M. Raman; generation of *scn4b* mutant mice, T.C. Bozza and S.T. Brown; experimental design of electrophysiology, H.V. White and I.M. Raman; experimentation, data collection, data analysis, qPCR, and genotyping, HVW; data interpretation and manuscript writing, H.V. White, T.C. Bozza, and I.M. Raman; comments and editing, S.T. Brown.

Submitted: 30 April 2019
Accepted: 3 September 2019

References

Afshari, F.S., K. Ptak, Z.M. Khaliq, T.M. Grieco, N.T. Slater, D.R. McCrimmon, and I.M. Raman. 2004. Resurgent Na currents in four classes of neurons of the cerebellum. *J. Neurophysiol.* 92:2831–2843. https://doi.org/10.1152/jn.00261.2004

Ahern, C.A., J. Payandeh, F. Bosmans, and B. Chanda. 2016. The hitchhiker's guide to the voltage-gated sodium channel galaxy. *J. Gen. Physiol.* 147:1–24. https://doi.org/10.1085/jgp.201511492

Ali, S., A. Shavkunov, N. Panova, S. Stoilova-McPhie, and F. Laezza. 2014. Modulation of the FGF14:FGF14 homodimer interaction through short peptide fragments. *CNS Neurol. Disord. Drug Targets.* 13:1559–1570. https://doi.org/10.2174/1871527313666141126103309

Ali, S.R., A.K. Singh, and F. Laezza. 2016. Identification of amino acid residues in fibroblast growth factor 14 (FGF14) required for structure-function interactions with voltage-gated sodium channel Nav1.6. *J. Biol. Chem.* 291:11268–11284. https://doi.org/10.1074/jbc.M115.703868

Aman, T.K., and I.M. Raman. 2007. Subunit dependence of Na channel slow inactivation and open channel block in cerebellar neurons. *Biophys. J.* 92:1938–1951. https://doi.org/10.1529/biophysj.106.093500

Aman, T.K., and I.M. Raman. 2010. Inwardly permeating Na ions generate the voltage dependence of resurgent Na current in cerebellar Purkinje neurons. *J. Neurosci.* 30:5629–5634. https://doi.org/10.1523/JNEUROSCI.0376-10.2010

Aman, T.K., T.M. Grieco-Calub, C. Chen, R. Rusconi, E.A. Slat, L.L. Isom, and I.M. Raman. 2009. Regulation of persistent Na current by interactions between beta subunits of voltage-gated Na channels. *J. Neurosci.* 29:2027–2042. https://doi.org/10.1523/JNEUROSCI.4531-08.2009

Bant, J.S., and I.M. Raman. 2010. Control of transient, resurgent, and persistent current by open-channel block by Na channel β4 in cultured cerebellar granule neurons. *Proc. Natl. Acad. Sci. USA.* 107:12357–12362. https://doi.org/10.1073/pnas.1005633107

Bant, J.S., T.K. Aman, and I.M. Raman. 2013. Antagonism of lidocaine inhibition by open-channel blockers that generate resurgent Na current. *J. Neurosci.* 33:4976–4987. https://doi.org/10.1523/JNEUROSCI.3026-12.2013

Barbosa, C., Z.Y. Tan, R. Wang, W. Xie, J.A. Strong, R.R. Patel, M.R. Vasko, J.M. Zhang, and T.R. Cummins. 2015. Navβ4 regulates fast resurgent sodium currents and excitability in sensory neurons. *Mol. Pain.* 11:60. https://doi.org/10.1186/s12990-015-0063-9

Barbosa, C., Y. Xiao, A.J. Johnson, W. Xie, J.A. Strong, J.M. Zhang, and T.R. Cummins. 2017. FHF2 isoforms differentially regulate Nav1.6-mediated resurgent sodium currents in dorsal root ganglion neurons. *Pflugers Arch.* 469:195–212. https://doi.org/10.1007/s00424-016-1911-9

Benton, M.D., A.H. Lewis, J.S. Bant, and I.M. Raman. 2013. Iberiotoxin-sensitive and -insensitive BK currents in Purkinje neuron somata. *J. Neurophysiol.* 109:2528–2541. https://doi.org/10.1152/jn.00127.2012

Berret, E., S.E. Kim, S.Y. Lee, C. Kushmerick, and J.H. Kim. 2016. Functional and structural properties of ion channels at the nerve terminal depends on compact myelin. *J. Physiol.* 594:5593–5609. https://doi.org/10.1113/JP272205

Bosch, M.K., Y. Carrasquillo, J.L. Ransdell, A. Kanakamedala, D.M. Ornitz, and J.M. Nerbonne. 2015. Intracellular FGF14 (iFGF14) is required for spontaneous and evoked firing in cerebellar Purkinje neurons and for motor coordination and balance. *J. Neurosci.* 35:6752–6769. https://doi.org/10.1523/JNEUROSCI.2663-14.2015

Buffington, S.A., and M.N. Rasband. 2013. Na+ channel-dependent recruitment of Navβ4 to axon initial segments and nodes of Ranvier. *J. Neurosci.* 33:6191–6202. https://doi.org/10.1523/JNEUROSCI.4051-12.2013

Bustin, S.A., V. Benes, J.A. Garson, J. Hellemans, J. Huggett, M. Kubista, R. Mueller, T. Nolan, M.W. Pfaffl, G.L. Shipley, et al. 2009. The MIQE guidelines: minimum information for publication of quantitative real-time PCR experiments. *Clin. Chem.* 55:611–622. https://doi.org/10.1373/clinchem.2008.112797

Campos, F.V., B. Chanda, P.S. Beirão, and F. Bezanilla. 2008. Alpha-scorpion toxin impairs a conformational change that leads to fast inactivation of muscle sodium channels. *J. Gen. Physiol.* 132:251–263. https://doi.org/10.1085/jgp.200809995

Capes, D.L., M.P. Goldschen-Ohm, M. Arcisio-Miranda, F. Bezanilla, and B. Chanda. 2013. Domain IV voltage-sensor movement is both sufficient and rate limiting for fast inactivation in sodium channels. *J. Gen. Physiol.* 142:101–112. https://doi.org/10.1085/jgp.201310998

Carter, B.C., and B.P. Bean. 2009. Sodium entry during action potentials of mammalian neurons: incomplete inactivation and reduced metabolic efficiency in fast-spiking neurons. *Neuron.* 64:898–909. https://doi.org/10.1016/j.neuron.2009.12.011

Carter, B.C., and B.P. Bean. 2011. Incomplete inactivation and rapid recovery of voltage-dependent sodium channels during high-frequency firing in cerebellar Purkinje neurons. *J. Neurophysiol.* 105:860–871. https://doi.org/10.1152/jn.01056.2010

Chen, Y., F.H. Yu, E.M. Sharp, D. Beacham, T. Scheuer, and W.A. Catterall. 2008. Functional properties and differential neuromodulation of Na(v) 1.6 channels. *Mol. Cell. Neurosci.* 38:607–615. https://doi.org/10.1016/j.mcn.2008.05.009

Clare, J.J., S.N. Tate, M. Nobbs, and M.A. Romanos. 2000. Voltage-gated sodium channels as therapeutic targets. *Drug Discov. Today.* 5:506–520. https://doi.org/10.1016/S1359-6446(00)01570-1

Di Re, J., P.A. Wadsworth, and F. Laezza. 2017. Intracellular fibroblast growth factor 14: Emerging risk factor for brain disorders. *Front. Cell. Neurosci.* 11:103. https://doi.org/10.3389/fncel.2017.00103

Do, M.T., and B.P. Bean. 2004. Sodium currents in subthalamic nucleus neurons from Nav1.6-null mice. *J. Neurophysiol.* 92:726–733. https://doi.org/10.1152/jn.00186.2004

Dover, K, S Solinas, E D'Angelo, and M Goldfarb. 2010. Long-term inactivation particle for voltage-gated sodium channels. *Journal of Physiology.* 588:3695–3711. https://doi.org/10.1113/jphysiol.2010.192559

Eaholtz, G., T. Scheuer, and W.A. Catterall. 1994. Restoration of inactivation and block of open sodium channels by an inactivation gate peptide. *Neuron.* 12:1041–1048. https://doi.org/10.1016/0896-6273(94)90312-3

El-Brolosy, M.A., and D.Y.R. Stainier. 2017. Genetic compensation: A phenomenon in search of mechanisms. *PLoS Genet.* 13:e1006780. https://doi.org/10.1371/journal.pgen.1006780

Goetz, R., K. Dover, F. Laezza, N. Shtraizent, X. Huang, D. Tchetchik, A.V. Eliseenkova, C.F. Xu, T.A. Neubert, D.M. Ornitz, et al. 2009. Crystal structure of a fibroblast growth factor homologous factor (FHF) defines a conserved surface on FHFs for binding and modulation of voltage-gated sodium channels. *J. Biol. Chem.* 284:17883–17896. https://doi.org/10.1074/jbc.M109.001842

Grieco, T.M., and I.M. Raman. 2004. Production of resurgent current in NaV1.6-null Purkinje neurons by slowing sodium channel inactivation with beta-pompilidotoxin. *J. Neurosci.* 24:35–42. https://doi.org/10.1523/JNEUROSCI.3807-03.2004

Grieco, T.M., F.S. Afshari, and I.M. Raman. 2002. A role for phosphorylation in the maintenance of resurgent sodium current in cerebellar Purkinje neurons. *J. Neurosci.* 22:3100–3107.

Grieco, T.M., J.D. Malhotra, C. Chen, L.L. Isom, and I.M. Raman. 2005. Open-channel block by the cytoplasmic tail of sodium channel beta4 as a mechanism for resurgent sodium current. *Neuron.* 45:233–244. https://doi.org/10.1016/j.neuron.2004.12.035

Hanck, D.A., and M.F. Sheets. 2007. Site-3 toxins and cardiac sodium channels. *Toxicon.* 49:181–193. https://doi.org/10.1016/j.toxicon.2006.09.017

Herzog, R.I., T.R. Cummins, F. Ghassemi, S.D. Dib-Hajj, and S.G. Waxman. 2003. Distinct repriming and closed-state inactivation kinetics of Nav1.6 and Nav1.7 sodium channels in mouse spinal sensory neurons. *J. Physiol.* 551:741–750. https://doi.org/10.1113/jphysiol.2003.047357

Hsu, W.-C.J., F. Scala, M.N. Nenov, N.C. Wildburger, H. Elferink, A.K. Singh, C.B. Chesson, T. Buzhdygan, M. Sohail, A.S. Shavkunov, et al. 2016. CK2 activity is required for the interaction of FGF14 with voltage-gated sodium channels and neuronal excitability. *FASEB J.* 30:2171–2186. https://doi.org/10.1096/fj.201500161

Kalume, F., F.H. Yu, R.E. Westenbroek, T. Scheuer, and W.A. Catterall. 2007. Reduced sodium current in Purkinje neurons from Nav1.1 mutant mice: implications for ataxia in severe myoclonic epilepsy in infancy. *J. Neurosci.* 27:11065–11074. https://doi.org/10.1523/JNEUROSCI.2162-07.2007

Khaliq, Z.M., N.W. Gouwens, and I.M. Raman. 2003. The contribution of resurgent sodium current to high-frequency firing in Purkinje neurons: an experimental and modeling study. *J. Neurosci.* 23:4899–4912. https://doi.org/10.1523/JNEUROSCI.23-12-04899.2003

Kim, J.H., C. Kushmerick, and H. von Gersdorff. 2010. Presynaptic resurgent Na+ currents sculpt the action potential waveform and increase firing reliability at a CNS nerve terminal. *J. Neurosci.* 30:15479–15490. https://doi.org/10.1523/JNEUROSCI.3982-10.2010

Kühn, F.J., and N.G. Greeff. 1999. Movement of voltage sensor S4 in domain 4 is tightly coupled to sodium channel fast inactivation and gating charge immobilization. *J. Gen.* Physiol. 114:167–183. https://doi.org/10.1085/jgp.114.2.167

Kuo, C.C., and B.P. Bean. 1994. Slow binding of phenytoin to inactivated sodium channels in rat hippocampal neurons. Mol. *Pharmacol.* 46:716–725.

Laezza, F., B.R. Gerber, J.Y. Lou, M.A. Kozel, H. Hartman, A.M. Craig, D.M. Ornitz, and J.M. Nerbonne. 2007. The FGF14(F145S) mutation disrupts the interaction of FGF14 with voltage-gated Na+ channels and impairs neuronal excitability. *J. Neurosci.* 27:12033–12044. https://doi.org/10.1523/JNEUROSCI.2282-07.2007

Laezza, F., A. Lampert, M.A. Kozel, B.R. Gerber, A.M. Rush, J.M. Nerbonne, S.G. Waxman, S.D. Dib-Hajj, and D.M. Ornitz. 2009. FGF14 N-terminal splice variants differentially modulate Nav1.2 and Nav1.6-encoded sodium channels. *Mol. Cell. Neurosci.* 42:90–101. https://doi.org/10.1016/j.mcn.2009.05.007

Lakso, M., J.G. Pichel, J.R. Gorman, B. Sauer, Y. Okamoto, E. Lee, F.W. Alt, and H. Westphal. 1996. Efficient in vivo manipulation of mouse genomic sequences at the zygote stage. *Proc. Natl. Acad. Sci. USA.* 93:5860–5865. https://doi.org/10.1073/pnas.93.12.5860

Lee, C.H., and P.C. Ruben. 2008. Interaction between voltage-gated sodium channels and the neurotoxin, tetrodotoxin. Channels (Austin). 2: 407–412. https://doi.org/10.4161/chan.2.6.7429

Levin, S.I., Z.M. Khaliq, T.K. Aman, T.M. Grieco, J.A. Kearney, I.M. Raman, and M.H. Meisler. 2006. Impaired motor function in mice with cell-specific knockout of sodium channel Scn8a (NaV1.6) in cerebellar purkinje neurons and granule cells. *J. Neurophysiol.* 96:785–793. https://doi.org/10.1152/jn.01193.2005

Lewis, A.H., and I.M. Raman. 2011. Cross-species conservation of open-channel block by Na channel β4 peptides reveals structural features required for resurgent Na current. *J. Neurosci.* 31:11527–11536. https://doi.org/10.1523/JNEUROSCI.1428-11.2011

Lewis, A.H., and I.M. Raman. 2013. Interactions among DIV voltage-sensor movement, fast inactivation, and resurgent Na current induced by the NaVβ4 open-channel blocking peptide. *J. Gen. Physiol.* 142:191–206. https://doi.org/10.1085/jgp.201310984

Lewis, A.H., and I.M. Raman. 2014. Resurgent current of voltage-gated Na(+) channels. *J. Physiol.* 592:4825–4838. https://doi.org/10.1113/jphysiol.2014.277582

Liu, C.j., S.D. Dib-Hajj, and S.G. Waxman. 2001. Fibroblast growth factor homologous factor 1B binds to the C terminus of the tetrodotoxin-resistant sodium channel rNav1.9a (NaN). *J. Biol. Chem.* 276: 18925–18933. https://doi.org/10.1074/jbc.M101606200

Lou, J.-Y., F. Laezza, B.R. Gerber, M. Xiao, K.A. Yamada, H. Hartmann, A.M. Craig, J.M. Nerbonne, and D.M. Ornitz. 2005. Fibroblast growth factor 14 is an intracellular modulator of voltage-gated sodium channels. *J. Physiol.* 569:179–193. https://doi.org/10.1113/jphysiol.2005.097220

Martina, M., A.E. Metz, and B.P. Bean. 2007. Voltage-dependent potassium currents during fast spikes of rat cerebellar Purkinje neurons: inhibition by BDS-I toxin. *J. Neurophysiol.* 97:563–571. https://doi.org/10.1152/jn.00269.2006

McPhee, J.C., D.S. Ragsdale, T. Scheuer, and W.A. Catterall. 1994. A mutation in segment IVS6 disrupts fast inactivation of sodium channels. *Proc. Natl. Acad. Sci. USA.* 91:12346–12350. https://doi.org/10.1073/pnas.91.25.12346

Mercer, J.N., C.S. Chan, T. Tkatch, J. Held, and D.J. Surmeier. 2007. Nav1.6 sodium channels are critical to pacemaking and fast spiking in globus pallidus neurons. *J. Neurosci.* 27:13552–13566. https://doi.org/10.1523/JNEUROSCI.3430-07.2007

Miyazaki, H., F. Oyama, R. Inoue, T. Aosaki, T. Abe, H. Kiyonari, Y. Kino, M. Kurosawa, J. Shimizu, I. Ogiwara, et al. 2014. Singular localization of sodium channel β4 subunit in unmyelinated fibres and its role in the striatum. *Nat. Commun.* 5:5525. https://doi.org/10.1038/ncomms6525

Moore, J.W., and T. Narahashi. 1967. Tetrodotoxin's highly selective blockage of an ionic channel. *Fed. Proc.* 26:1655–1663.

Motoike, H.K., H. Liu, I.W. Glaaser, A.S. Yang, M. Tateyama, and R.S. Kass. 2004. The Na+ channel inactivation gate is a molecular complex: a novel role of the COOH-terminal domain. *J. Gen. Physiol.* 123:155–165. https://doi.org/10.1085/jgp.200308929

Munoz-Sanjuan, I., P.M. Smallwood, and J. Nathans. 2000. Isoform diversity among fibroblast growth factor homologous factors is generated by alternative promoter usage and differential splicing. *J. Biol. Chem.* 275: 2589–2597. https://doi.org/10.1074/jbc.275.4.2589

Pablo, J.L., and G.S. Pitt. 2016. Fibroblast growth factor homologous factors: New roles in neuronal health and disease. *Neuroscientist.* 22:19–25. https://doi.org/10.1177/1073858414562217

Pablo, J.L., C. Wang, M.M. Presby, and G.S. Pitt. 2016. Polarized localization of voltage-gated Na+ channels is regulated by concerted FGF13 and FGF14 action. *Proc. Natl. Acad. Sci. USA.* 113:E2665–E2674. https://doi.org/10.1073/pnas.1521194113

Pan, X., Z. Li, Q. Zhou, H. Shen, K. Wu, X. Huang, J. Chen, J. Zhang, X. Zhu, J. Lei, et al. 2018. Structure of the human voltage-gated sodium channel $Na_v1.4$ in complex with β1. *Science.* 362:eaau2486. https://doi.org/10.1126/science.aau2486

Raman, I.M., and B.P. Bean. 1997. Resurgent sodium current and action potential formation in dissociated cerebellar Purkinje neurons. *J. Neurosci.* 17:4517–4526. https://doi.org/10.1523/JNEUROSCI.17-12-04517.1997

Raman, I.M., and B.P. Bean. 1999. Ionic currents underlying spontaneous action potentials in isolated cerebellar Purkinje neurons. *J. Neurosci.* 19: 1663–1674. https://doi.org/10.1523/JNEUROSCI.19-05-01663.1999

Raman, I.M., and B.P. Bean. 2001. Inactivation and recovery of sodium currents in cerebellar Purkinje neurons: evidence for two mechanisms. *Biophys. J.* 80:729–737. https://doi.org/10.1016/S0006-3495(01)76052-3

Raman, I.M., L.K. Sprunger, M.H. Meisler, and B.P. Bean. 1997. Altered subthreshold sodium currents and disrupted firing patterns in Purkinje neurons of Scn8a mutant mice. *Neuron.* 19:881–891. https://doi.org/10.1016/S0896-6273(00)80969-1

Ransdell, J.L., E. Dranoff, B. Lau, W.L. Lo, D.L. Donermeyer, P.M. Allen, and J.M. Nerbonne. 2017. Loss of Navβ4-mediated regulation of sodium currents in adult Purkinje neurons disrupts firing and impairs motor coordination and balance. *Cell Reports.* 19:532–544. https://doi.org/10.1016/j.celrep.2017.03.068

Rosker, C., B. Lohberger, D. Hofer, B. Steinecker, S. Quasthoff, and W. Schreibmayer. 2007. The TTX metabolite 4,9-anhydro-TTX is a highly specific blocker of the Na(v1.6) voltage-dependent sodium channel. *Am. J. Physiol. Cell Physiol.* 293:C783–C789. https://doi.org/10.1152/ajpcell.00070.2007

Schaller, K.L., and J.H. Caldwell. 2003. Expression and distribution of voltage-gated sodium channels in the cerebellum. *Cerebellum.* 2:2–9. https://doi.org/10.1080/14734220309424

Schiavon, E., T. Sacco, R.R. Cassulini, G. Gurrola, F. Tempia, L.D. Possani, and E. Wanke. 2006. Resurgent current and voltage sensor trapping enhanced activation by a beta-scorpion toxin solely in Nav1.6 channel. Significance in mice Purkinje neurons. *J. Biol. Chem.* 281:20326–20337. https://doi.org/10.1074/jbc.M600565200

Shakkottai, V.G., M. Xiao, L. Xu, M. Wong, J.M. Nerbonne, D.M. Ornitz, and K.A. Yamada. 2009. FGF14 regulates the intrinsic excitability of cerebellar Purkinje neurons. *Neurobiol. Dis.* 33:81–88. https://doi.org/10.1016/j.nbd.2008.09.019

Shen, H., D. Liu, K. Wu, J. Lei, and N. Yan. 2019. Structures of human $Na_v1.7$ channel in complex with auxiliary subunits and animal toxins. *Science.* 363:1303–1308. https://doi.org/10.1126/science.aaw2493

Skarnes, W.C., B. Rosen, A.P. West, M. Koutsourakis, W. Bushell, V. Iyer, A.O. Mujica, M. Thomas, J. Harrow, T. Cox, et al. 2011. A conditional knockout resource for the genome-wide study of mouse gene function. *Nature.* 474:337–342. https://doi.org/10.1038/nature10163

Smith, M.R., R.D. Smith, N.W. Plummer, M.H. Meisler, and A.L. Goldin. 1998. Functional analysis of the mouse Scn8a sodium channel. *J. Neurosci.* 18: 6093–6102. https://doi.org/10.1523/JNEUROSCI.18-16-06093.1998

Tang, L., R.G. Kallen, and R. Horn. 1996. Role of an S4-S5 linker in sodium channel inactivation probed by mutagenesis and a peptide blocker. *J. Gen. Physiol.* 108:89–104. https://doi.org/10.1085/jgp.108.2.89

Theile, J.W., B.W. Jarecki, A.D. Piekarz, and T.R. Cummins. 2011. Nav1.7 mutations associated with paroxysmal extreme pain disorder, but not erythromelalgia, enhance Navbeta4 peptide-mediated resurgent sodium currents. *J. Physiol.* 589:597–608. https://doi.org/10.1113/jphysiol.2010.200915

Turrigiano, G.G. 2008. The self-tuning neuron: synaptic scaling of excitatory synapses. *Cell.* 135:422–435. https://doi.org/10.1016/j.cell.2008.10.008

Wang, Q., D.G. McEwen, and D.M. Ornitz. 2000. Subcellular and developmental expression of alternatively spliced forms of fibroblast growth factor 14. *Mech. Dev.* 90:283–287. https://doi.org/10.1016/S0925-4773(99)00241-5

Wang, Q., M.E. Bardgett, M. Wong, D.F. Wozniak, J. Lou, B.D. McNeil, C. Chen, A. Nardi, D.C. Reid, K. Yamada, and D.M. Ornitz. 2002. Ataxia and paroxysmal dyskinesia in mice lacking axonally transported FGF14. *Neuron.* 35:25–38. https://doi.org/10.1016/S0896-6273(02)00744-4

Wang, S.Y., K. Bonner, C. Russell, and G.K. Wang. 2003. Tryptophan scanning of D1S6 and D4S6 C-termini in voltage-gated sodium channels. *Biophys. J.* 85:911–920. https://doi.org/10.1016/S0006-3495(03)74530-5

Warming, S., N. Costantino, D.L. Court, N.A. Jenkins, and N.G. Copeland. 2005. Simple and highly efficient BAC recombineering using galK selection. *Nucleic Acids Res.* 33:e36. https://doi.org/10.1093/nar/gni035

West, J.W., D.E. Patton, T. Scheuer, Y. Wang, A.L. Goldin, and W.A. Catterall. 1992. A cluster of hydrophobic amino acid residues required for fast Na(+)-channel inactivation. *Proc. Natl. Acad. Sci. USA.* 89:10910–10914. https://doi.org/10.1073/pnas.89.22.10910

Xiao, M., M.K. Bosch, J.M. Nerbonne, and D.M. Ornitz. 2013. FGF14 localization and organization of the axon initial segment. *Mol. Cell. Neurosci.* 56:393–403. https://doi.org/10.1016/j.mcn.2013.07.008

Xie, W., Z.Y. Tan, C. Barbosa, J.A. Strong, T.R. Cummins, and J.M. Zhang. 2016. Upregulation of the sodium channel NaVβ4 subunit and its contributions to mechanical hypersensitivity and neuronal hyperexcitability in a rat model of radicular pain induced by local dorsal root ganglion inflammation. *Pain.* 157:879–891. https://doi.org/10.1097/j.pain.0000000000000453

Yan, H., J.L. Pablo, C. Wang, and G.S. Pitt. 2014. FGF14 modulates resurgent sodium current in mouse cerebellar Purkinje neurons. *eLife.* 3:e04193. https://doi.org/10.7554/eLife.04193

Yan, Z., Q. Zhou, L. Wang, J. Wu, Y. Zhao, G. Huang, W. Peng, H. Shen, J. Lei, and N. Yan. 2017. Structure of the Nav1.4-beta1 Complex from Electric Eel. *Cell.* 170:470–482.e411. https://doi.org/10.1016/j.cell.2017.06.039

Yang, N., and R. Horn. 1995. Evidence for voltage-dependent S4 movement in sodium channels. *Neuron.* 15:213–218. https://doi.org/10.1016/0896-6273(95)90078-0

Yap, E.L., and M.E. Greenberg. 2018. Activity-regulated transcription: Bridging the gap between neural activity and behavior. *Neuron.* 100: 330–348. https://doi.org/10.1016/j.neuron.2018.10.013

Yu, F.H., R.E. Westenbroek, I. Silos-Santiago, K.A. McCormick, D. Lawson, P. Ge, H. Ferriera, J. Lilly, P.S. DiStefano, W.A. Catterall, et al. 2003. Sodium channel beta4, a new disulfide-linked auxiliary subunit with similarity to beta2. *J. Neurosci.* 23:7577–7585. https://doi.org/10.1523/JNEUROSCI.23-20-07577.2003